RSC Applied Polymers

ROYAL SOCIETY OF CHEMISTRY

PERSPECTIVE

View Article Online
View Journal

Cite this: DOI: 10.1039/d6lp00044d

Polymersomes with aggregation-induced emission: synthesis, self-assembly, and biomedical applications

Yubin Pu,[a] Hao Han,[a] Siyu Song*[b] and Shoupeng Cao *[a]

Polymeric vesicles, also known as polymersomes, are self-assembled nanostructures typically from amphiphilic block copolymers. They have been regarded as versatile platforms with broad biomedical applications owing to their facile ability to modulate their chemical structure, tunable membrane properties, and high cargo-loading capacity. The integration of aggregation-induced emission (AIE) luminogens into polymersomes has emerged as a powerful strategy to overcome the disadvantageous effects of conventional fluorophores, such as aggregation-induced quenching and photobleaching. This enables AIE-active polymersomes to exhibit bright fluorescence, enhanced photostability, and multifunctionality in complex biological environments. In this review, we discuss recent advances in AIE-active polymersomes, with an emphasis on their molecular design, self-assembly behaviors, and biomedical applications. We highlight how precise control over polymer composition, block architecture, and AIEgen incorporation governs vesicle formation, size, morphology, membrane properties, and function. The emerging biomedical applications of AIE-active polymersomes are then summarized, including bioimaging, catalysis, drug delivery, photodynamic therapy, and theranostics, highlighting the synergistic integration of imaging and therapeutic functions. Finally, current challenges and future perspectives are discussed, particularly regarding biodegradability and stimulus responsiveness of next-generation AIE-active polymersomes for advanced biomedical applications and clinical translation.

Received 6th February 2026,
Accepted 8th April 2026

DOI: 10.1039/d6lp00044d

rsc.li/rscapplpolym

Introduction

Inspired by the hierarchical organization and compartmentalization in natural systems, the self-assembly of amphiphilic block copolymers (BCPs) has emerged as a powerful and versatile strategy for constructing functional nanomaterials.[1–5] Over the past decades, remarkable advances in molecular design and controlled polymerization techniques—such as reversible addition–fragmentation chain transfer (RAFT), atom transfer radical polymerization (ATRP), and ring-opening polymerization (ROP)—have enabled unprecedented control over polymer composition, molecular weight, block ratio, and architecture.[6–10] These developments allow amphiphilic block copolymers to be precisely tailored at the molecular level, providing a robust toolbox for the rational design of nanoscale assemblies with predictable structures and properties. Fine-tuning parameters, including polymer composition, molecular weight, amphiphilicity, charge density, and polydispersity index, enables the facile formation of a wide range of polymeric nano-architectures.[11,12] These include spherical micelles, cylindrical or worm-like micelles, lamellae, bilayer vesicles, and inverse mesophases, each exhibiting distinct structural and functional characteristics.[13–16] Importantly, the physical and chemical properties of BCP-based assemblies—such as size, morphology, mechanical stability, surface chemistry, membrane flexibility, and responsiveness to environmental stimuli—can be readily adjusted to meet the requirements of diverse technological and biomedical applications.[17–21] This structural diversity, combined with superior stability compared to small-molecule surfactant systems, has positioned polymeric self-assemblies as a cornerstone of modern soft matter and nanomedicine research.[22–24]

Among the polymeric assemblies, polymersomes attract enormous interest from the scientific community due to their unique bilayer membrane architecture that closely resembles biological compartments.[25] Polymersomes typically exhibit sizes in the nanometer range (approximately 30–1000 nm), making them well-suited for nanoscale biomedical applications.[22,26–28] Notably, by adjusting polymer composition, molecular weight, and assembly conditions, polymersomes with micrometer-scale dimensions

[a]College of Polymer Science and Engineering, National Key Laboratory of Advanced Polymer Materials, Sichuan University, Chengdu 610065, PR China. E-mail: caoshoupeng@scu.edu.cn
[b]Life-Like Materials and Systems, Department of Chemistry, University of Mainz, 55128 Mainz, Germany. E-mail: siyu.song@uni-mainz.de

(1–100 μm), comparable to living cells, can also be obtained.[29,30] This size tunability, together with their robust membrane structure, enables polymersomes to serve as versatile platforms for mimicking biological compartments and constructing cell-like systems.[31] One of the most attractive features of polymersomes lies in their intrinsic compartmentalization capability. Their hydrophobic bilayer membrane can accommodate hydrophobic species such as emissive agents, photosensitizers, and small-molecule drugs, while the aqueous lumen provides a confined environment for encapsulating hydrophilic cargoes, including enzymes, proteins, DNA, and RNA. This dual-loading capacity, combined with enhanced mechanical stability, has enabled polymersomes to find widespread applications across physics, materials science, and nanomedicine.[32–35] From an optical perspective, the polymersomes can serve as versatile platforms for fluorescence imaging, sensing, and light-harvesting by embedding chromophores or fluorescent polymers within their membranes or cavities.[36] In addition, polymer vesicles can also be engineered to participate in photochemical (such as photocatalysis and light-triggered release) and photothermal processes through the integration of photosensitive or catalytic moieties.[37–39] In biomedical contexts, polymersomes have been extensively explored as carriers for drug delivery, platforms for artificial cells, nanoreactors for biocatalysis, and multifunctional theranostic agents.[40–44] In these applications, fluorescence imaging plays an indispensable role.[45,46] Fluorescent labelling enables real-time visualization of polymersome formation, tracking of their biodistribution, monitoring of cellular uptake and intracellular trafficking, and evaluation of therapeutic responses *in vitro* and *in vivo*.[47,48] However, conventional imaging agents, including small-molecule organic dyes, fluorescent proteins, and inorganic nanoprobes such as quantum dots, often suffer from inherent limitations when applied in polymeric assemblies. Organic dyes typically exhibit aggregation-caused quenching (ACQ), leading to severe fluorescence loss when confined within polymer membranes or loaded at high concentrations.[49–51] Fluorescent proteins face issues related to limited photostability and sensitivity to environmental conditions, while inorganic probes may introduce concerns regarding cytotoxicity, long-term biocompatibility, and complex surface modification.[52–54] These drawbacks significantly restrict the performance and reliability of traditional fluorophores in polymersome-based biomedical systems.

To overcome these challenges, the concept of aggregation-induced emission (AIE) has emerged as a paradigm-shifting strategy in the field of luminescent materials.[55] In contrast to conventional fluorophores, AIE-active molecules are weakly emissive or non-emissive in dilute solution but exhibit intense fluorescence upon aggregation or confinement.[56,57] This unique behavior is generally attributed to the restriction of intramolecular motions, which suppresses non-radiative decay pathways in the aggregated state.[58,59] As a result, AIE luminogens (AIEgens) display several key merits, including high fluorescence brightness in condensed phases, excellent photostability, large Stokes shifts, and resistance to self-quenching. These features make AIEgens particularly attractive for biological imaging, where fluorophores frequently operate in crowded, heterogeneous, and dynamically changing environments.[60–62] The smart integration of AIE with polymersomes offers a compelling solution to the longstanding challenges associated with fluorescence imaging in polymeric vesicle systems.[63] By leveraging the aggregation-tolerant emission behavior of AIEgens and the structural confinement provided by polymersomes, it becomes possible to construct highly emissive, stable, and multifunctional nanostructures. Importantly, polymersomes provide an ideal platform for activating AIE behavior, as the hydrophobic membrane or confined interior naturally promotes aggregation or restriction of molecular motion, thereby enhancing emission efficiency.[64]

Various design strategies have been explored to integrate aggregation-induced emission (AIE) functionality into polymersomes, among which chemical conjugation of AIE luminogens (AIEgens) with polymeric systems has emerged as the most robust and versatile approach.[65] In this strategy, AIEgens are covalently tethered to polymer backbones or side chains or incorporated as integral segments within amphiphilic block copolymers that subsequently self-assemble into vesicular architectures. Compared with physical encapsulation methods —which often suffer from dye leakage, limited loading stability, and poor control over spatial distribution—chemical conjugation ensures precise localization of AIEgens within the polymersome membrane, enhanced structural stability, and long-term retention of emissive functionality.[66] Moreover, the molecular integration of AIEgens enables fine regulation of emission behavior through polymer composition, block architecture, and self-assembly conditions. Beyond fluorescence imaging, covalently incorporated AIEgens can impart additional functionalities, including stimulus-responsive fluorescence modulation, efficient reactive oxygen species generation for photodynamic therapy, and tightly coupled imaging–therapy integration.[67–69] Through rational molecular design and controlled self-assembly, chemically AIE-functionalized polymersomes allow precise control over vesicle size, morphology, membrane permeability, and photophysical properties, thereby significantly expanding the functional scope of polymersomes for advanced biomedical applications.

In this review, we provide a comprehensive overview of recent advances in polymersomes integrated with aggregation-induced emission (Scheme 1). We first summarize the mole-

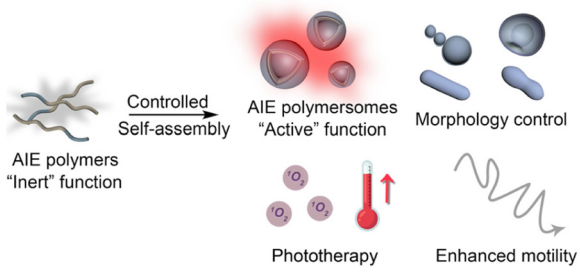

Scheme 1 Schematic illustration of engineering active polymersomes with aggregation-induced emission.

cular design principles and synthetic strategies for constructing AIE-active amphiphilic block copolymers and their self-assembly into vesicular nanostructures. We then discuss how polymer composition, architecture, and assembly conditions influence the structural and photophysical properties of AIE-functionalized polymersomes. Subsequently, we highlight representative biomedical applications, including fluorescence imaging, controlled drug delivery, photodynamic therapy, and multifunctional theranostics. Finally, we discuss current challenges and future perspectives, with a focus on biodegradability, stimulus responsiveness, mechanistic understanding, and translational potential. Through this review, we aim to provide design guidelines and conceptual insights that will inspire the development of next-generation AIE-based polymersomes for advanced biomedical applications.

Construction of AIE-active polymersomes

Synthetic approach for AIE-active polymersomes

Most AIE-active polymersomes reported to date have been constructed from the self-assembly of amphiphilic block copolymers, in which incorporation of AIE luminogens represents the essential prerequisite for building multifunctional polymeric vesicles.[70] Several controlled polymerization strategies have proven particularly effective for preparing AIE-containing amphiphilic block copolymers, most notably RAFT (reversible addition–fragmentation chain-transfer polymerization), ATRP (atom-transfer radical polymerization), and metal-free ROP (ring-opening polymerization) of aliphatic polycarbonates.[71] Each route offers distinct advantages in terms of monomer scope, architectural complexity, and polymer chain precision, enabling tailored access to functional block copolymers for diverse applications.

Among these methods, RAFT polymerization stands out as a highly versatile platform for constructing amphiphilic block polymers with well-defined molecular weights and narrow dispersities.[72–74] Owing to its broad monomer tolerance and compatibility with functional groups, RAFT facilitates the modular incorporation of various AIE luminogens into block architectures. For example, He *et al*. reported the synthesis of poly(*N*-(2-methacryloyloxyethyl)-pyrrolidone)-*b*-poly(lauryl methacrylate-*co*-1-ethenyl-4-(1,2,2-triphenylethenyl)benzene) *via* a two-step RAFT process, which enabled the ordered distribution of hydrophilic (NMP, *N*-(2-methacryloyloxyethyl)pyrrolidone) and hydrophobic (LMA, lauryl methacrylate/TPE, 1,1,2,2-tetraphenylethylene) segments with narrow dispersities (PDI ~ 1.10, Fig. 1a).[75] Notably, precise control over the hydrophobic block length allowed the authors to modulate the resulting self-assembly morphology from spherical nanoparticles to worm-like structures, highlighting the sensitivity of the AIE polymersome morphology to the hydrophilic/hydrophobic balance. Beyond block architectures, RAFT polymerization also enables the generation of random amphiphilic copolymers featuring intrinsic fluorescence. Wei *et al.* synthesized PEG-based

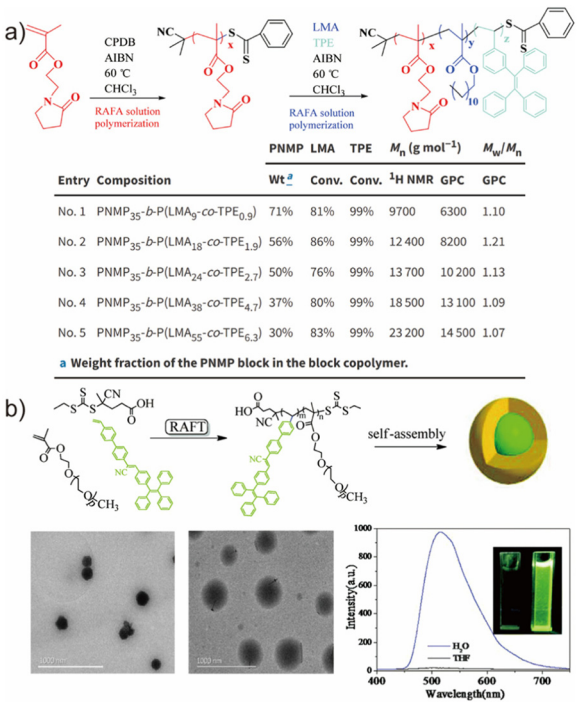

Entry	Composition	PNMP Wt[a]	LMA Conv.	TPE Conv.	M_n (^{1}H NMR)	M_n GPC	M_w/M_n GPC
No. 1	$PNMP_{35}$-*b*-P(LMA_9-*co*-$TPE_{0.9}$)	71%	81%	99%	9700	6300	1.10
No. 2	$PNMP_{35}$-*b*-P(LMA_{18}-*co*-$TPE_{1.9}$)	56%	86%	99%	12 400	8200	1.21
No. 3	$PNMP_{35}$-*b*-P(LMA_{24}-*co*-$TPE_{2.7}$)	50%	76%	99%	13 700	10 200	1.13
No. 4	$PNMP_{35}$-*b*-P(LMA_{38}-*co*-$TPE_{4.7}$)	37%	80%	99%	18 500	13 100	1.09
No. 5	$PNMP_{35}$-*b*-P(LMA_{55}-*co*-$TPE_{6.3}$)	30%	83%	99%	23 200	14 500	1.07

a Weight fraction of the PNMP block in the block copolymer.

Fig. 1 (a) The scheme of synthesizing the AIEgenic copolymer (PNMPx-*b*-P(LMAy-*co*-TPEz)) *via* RAFT polymerization and the summary of the molecular weight and PDI of these block copolymers. Adapted with permission under a Creative Commons CC BY-NC license from ref. 75. Copyright 2019 Royal Society of Chemistry. (b) The synthetic route of the PEG-TS polymers *via* RAFT polymerization, the self-assembly results (*via* TEM), and the AIE phenomenon of this copolymer. Adapted with permission from ref. 76. Copyright 2019 Royal Society of Chemistry.

methacrylate copolymers bearing TPE moieties in a single-step RAFT process using a carboxyl-terminated chain transfer agent (CTA) and 2,2′-azobis(2-methylpropionitrile) (AIBN) initiator, affording polymers with narrow dispersities (PDI ~ 1.26, Fig. 1b).[76] These examples underscore that RAFT polymerization, through its ability to regulate block composition, chain length, and monomer sequence, provides a powerful handle to dissect the structure–assembly relationships governing AIE-active amphiphilic polymers and their vesicular morphologies.

In addition to RAFT strategies, atom transfer radical polymerization (ATRP) represents another widely employed route for synthesizing well-defined AIE-active amphiphilic copolymers.[77,78] A notable example was reported by Wei *et al.*, who prepared AIE-containing copolymers *via* metal-free photomediated ATRP under 380 nm irradiation using 2-methacryloyloxyethyl phosphorylcholine (MPC) and benzyl methacrylate (BzMA) as monomers (Fig. 2a).[79] In contrast to conventional ATRP, the system employed 10-phenylphenothiazine (PTH) as a photocatalytic chain-transfer agent, enabling reversible activation–deactivation cycles without the need for metal catalysts. The room-temperature, metal-free conditions greatly simplify post-polymerization purification and reduce environmental burdens associated with metal residues and heating. The resulting amphiphilic copolymers exhibited dispersities of

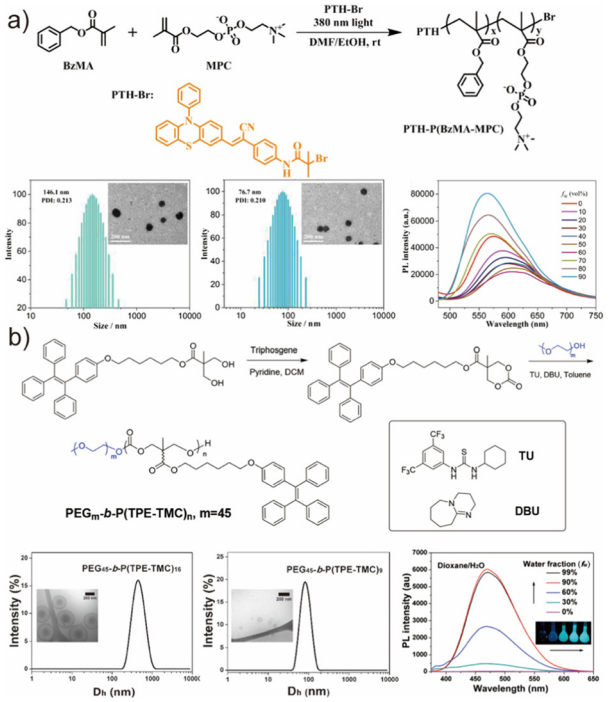

Fig. 2 (a) Schematic showing the synthesis of PTH-P(BzMA-MPC) *via* ATRP, the size distribution and morphology (*via* DLS and TEM), followed by displaying the AIE phenomenon. Adapted with permission from ref. 79. Copyright 2020 Elsevier. (b) Synthetic route of the AIEgenic copolymer PEG45-*b*-P(TPE-TMC)$_n$ *via* ROP, self-assembly outcomes (*via* TEM) and the AIE phenomenon of this copolymer. Adapted with permission from ref. 80. Copyright 2018 America Chemical Society.

1.52 and 1.48 for PTH-P(BzMA-MPC)-20 and PTH-P(BzMA-MPC)-40, respectively, and formed nanoparticles with sizes dependent on the hydrophilic/hydrophobic segment ratio. Although the obtained dispersities were relatively broad, this work highlights a convenient and environmentally benign pathway for constructing AIE-active amphiphilic copolymers with intrinsic fluorescence.

For biological applications of AIE-active polymeric assemblies, a key requirement lies in achieving biocompatibility and non-toxic degradation under physiological conditions.[81,82] This has motivated increasing interest in amphiphilic block copolymers based on degradable carbonate backbones. Poly(ethylene glycol)-*block*-poly(trimethylene carbonate) (PEG-PTMC) represents a representative platform, offering biodegradability, modular composition, and facile functionalization.[83,84] Importantly, unlike polyester analogues, PTMC degrades *via* surface erosion without generating acidic by-products or relying on enzymatic catalysis—properties that are advantageous for biomedical deployment. Controlled ring-opening polymerization (ROP) of trimethylene carbonate (TMC) enables the synthesis of PTMC-based copolymers with precise molecular weights, tailored hydrophilic/hydrophobic ratios, and well-defined end-group chemistry using organometallic or organic catalytic systems. Li *et al.* provided a representative example by constructing a family of AIE-active amphiphilic block copolymers through organocatalytic ROP (Fig. 2b).[80] PEG$_{45}$–OH served as a macro-initiator, while a tetraphenyl-ethylene-functionalized cyclic carbonate (TPE-TMC) monomer was polymerized in the presence of *N*-(3,5-bis(trifluoromethyl)phenyl)-*N*′-cyclohexylthiourea (TU) and 1,8-diazabicyclo [5.4.0]undec-7-ene (DBU). The resulting copolymers displayed well-controlled molecular characteristics and a pronounced AIE behavior, as the emission was quenched in pure THF or dioxane and significantly enhanced upon water addition. Solvent-switch assembly yielded fluorescent polymersomes in aqueous media, where vesicle formation restricted intramolecular rotations of the pendant TPE groups. Notably, decreasing the hydrophobic block length reduced the vesicle size from approximately 450 nm to 70 nm, illustrating how the precision of ROP enables systematic control over self-assembly dimensions. The combination of biodegradability, biocompatibility, and tunable nanoscale morphology renders carbonate-based AIE polymersomes promising candidates for biomedical applications.

In summary, the synthesis of AIE-active polymers for polymersomes has primarily focused on controlling block copolymer composition, functional group incorporation, and polymer chain length to tune self-assembly and photophysical

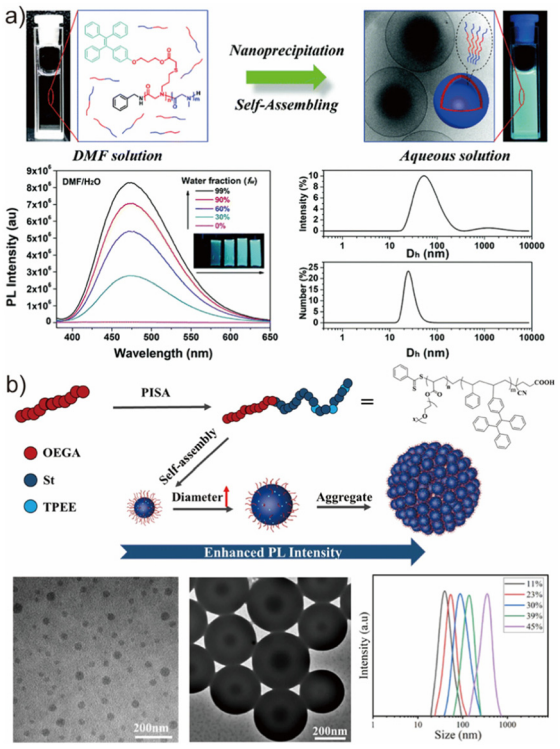

Fig. 3 (a) Schematic diagram of the self-assembly of P(TPE-NAG)-*b*-PSar in aqueous solution, the AIE phenomenon of the polymersome dispersion and size distribution of these nanoparticles. Adapted with permission from ref. 87. Copyright 2019 Royal Society of Chemistry. (b) Illustration of the evolution of self-assembly morphologies and the increase of PL intensity during the RAFT-PISA process, followed by the TEM figure and DLS chart proving this variation. Adapted with permission from ref. 88. Copyright 2022 Springer Nature.

properties. Moving forward, future efforts may involve the development of more versatile and modular synthetic strategies, enabling precise control over AIEgen placement, density, and responsive functionalities. Such advances are expected to facilitate more predictable structure–property relationships and expand the scope of optoelectronic and biomedical applications.

Self-assembly methods of the polymersomes with aggregation-induced emission

A widely employed strategy for preparing nanoscale AIE-active polymersomes is the solvent-switch (nanoprecipitation) method, which leverages the limited water solubility of most amphiphilic copolymers.[70,85,86] In this approach, copolymers are first dissolved in a polar organic solvent such as *N*,*N*-dimethylformamide (DMF) or tetrahydrofuran (THF), followed by gradual addition of water as the selective solvent to induce copolymer self-assembly and vesicle formation. The process can also be performed inversely by adding the polymer solution to water. Subsequent dialysis is generally required to remove the residual organic solvent, especially for biological applications. For example, Li *et al.* prepared AIE-active polymersomes through nanoprecipitation using DMF/water mixtures (Fig. 3a).[87] A solution of AIE-bearing copolymer in DMF was combined with water at a controlled injection rate (2.5 μL min^{-1}) followed by exhaustive dialysis, yielding polymersomes whose size distribution and morphology were characterized by DLS and cryo-EM. Although the solvent-switch method affords polymeric vesicles with well-defined dimensions and morphologies, its practical limitations—including the need for slow solvent exchange, dialysis, and relatively high solvent consumption—have motivated the development of more efficient *in situ* assembly strategies.

Polymerization-induced self-assembly (PISA) has emerged as a powerful alternative enabling the direct synthesis and assembly of amphiphilic block copolymers in a single step.[89,90] Benefiting from controlled polymerization techniques described above, PISA enables high solid content, scalable production, and tunable nanoparticle morphologies, and has therefore attracted considerable interest for fabricating AIE-active nanostructures.[91,92] In 2022, Pang *et al.* reported the preparation of AIE-active nanoparticles *via* photo-initiated PISA (Fig. 3b).[88] A POEGA macro-CTA was first synthesized by RAFT polymerization using AIBN as an initiator and CPADB as a chain transfer agent. Subsequent dispersion polymerization in ethanol produced amphiphilic block copolymers bearing TPE-based side groups, where the monomers remained soluble but the growing block phase-separated to drive *in situ* self-assembly under UV irradiation without an additional initiator. Interestingly, the increase in monomer conversion correlated with enhanced fluorescence emission of the TPE moieties, reflecting progressively restricted intramolecular motion during nanoparticle growth. The fluorescence intensity and particle size scaled with conversion, illustrating that AIE provides an intrinsic and convenient signal to monitor PISA in real time. Compared with solvent-switch methods, PISA enables efficient, scalable, and high-solid-content preparation of AIE-active nanoparticles, making it particularly attractive for the mass production of functional fluorescent polymeric nanostructures.

Morphology control of AIE-active polymersomes

Amphiphilic block copolymers readily self-assemble in aqueous media into a rich spectrum of morphologies—including spherical micelles, cylindrical micelles, vesicles, stomatocytes, and other higher-order structures—driven primarily by the interplay between hydrophilic solvation and hydrophobic association, which minimizes interfacial energy and system free energy.[19,93,94] Accordingly, the relative volume fractions of the hydrophilic and hydrophobic segments represent an effective and widely adopted handle for morphology regulation.[14,95,96] Beyond the mechanistic understanding, controlling the morphology of polymersomes is of fundamental importance, as their shape and membrane structure play a crucial role in determining their physicochemical properties and potential applications. Li *et al.* synthesized poly(ethylene glycol)-*b*-poly[(2-(diethylamino)ethyl methacrylate)-*co*-(tetraphenylethene functionalized methacrylate)] (PEG-*b*-P

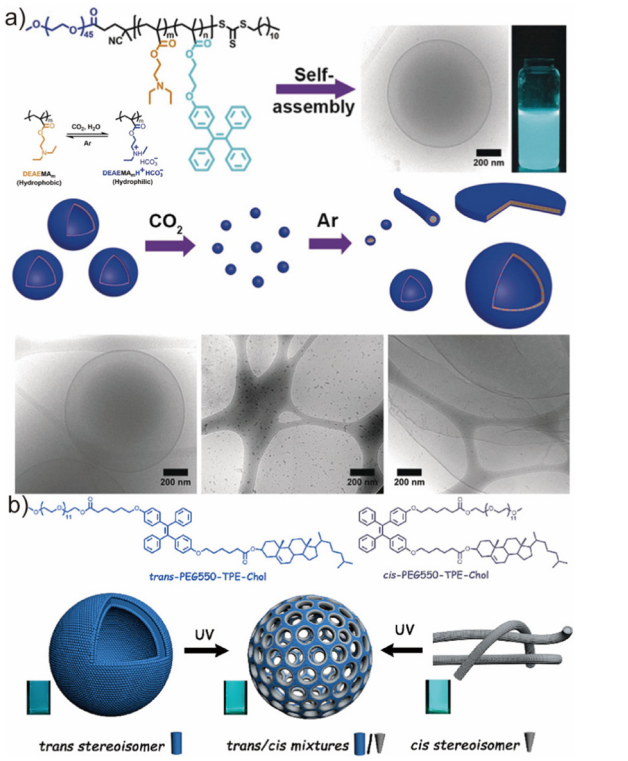

Fig. 4 (a) The scheme of CO_2 and Ar responsive self-assembly of the copolymer PEG-*b*-P(DEAEMA-*co*-TPEMA) into AIE fluorescent polymersomes and the cryo-TEM image indicated the changes in the morphology of these nano-assemblies. Adapted with permission from ref. 97. Copyright 2021 Wiley. (b) The scheme of the light-gated nano-porous capsules from stereoisomer-directed self-assemblies. Adapted with permission from ref. 98. Copyright 2021 America Chemical Society.

(DEAEMA-*co*-TPEMA)) *via* RAFT polymerization and subsequently obtained CO_2-responsive AIE-active vesicles through nanoprecipitation in THF/water and dioxane/water mixtures (Fig. 4a).[97] In this copolymer, DEAEMA and TPEMA served as the hydrophobic components, whereas PEG constituted the hydrophilic block. Upon CO_2 bubbling, protonation of DEAEMA reversed its hydrophobicity, triggering a vesicle-to-micelle transition. Subsequent Ar bubbling restored the original hydrophobic/hydrophilic balance and induced micelle-to-vesicle reformation. This reversible morphology switching highlights the potential of AIE-active vesicles as dynamic nanostructures responsive to gaseous stimuli.

Beyond segmental composition, alterations in molecular stereochemistry provide an orthogonal means to modulate the self-assembly behavior of AIE-bearing copolymers. In 2021, Li *et al.* reported stereoisomer-directed assemblies of UV-responsive, structure-inherent fluorescent AIE copolymers containing PEG550-TPE-cholesterol motifs (Fig. 4b).[98] Strikingly, pure *trans*-PEG550-TPE-Chol assembled into spherical vesicles, whereas the *cis* isomer formed cylindrical micelles; copolymers with a mixed stereoisomer composition (*trans*/*cis* ≈ 60/40) yielded porous vesicles featuring membrane pores of 9–27 nm. Stereochemistry also affected emission behavior, with the *cis* isomer exhibiting stronger fluorescence intensity relative to the *trans* and mixed species. Photochemical *cis* ↔ *trans* interconversion could be induced under intense UV irradiation (15 mW cm^{-2}), altering both self-assembly morphology and fluorescence output (apparently different PL intensity between *trans* and *cis* self-assemblies). In a theoretical perspective, membrane mechanical properties, such as flexibility and curvature, can influence the packing and mobility of embedded AIEgens, thereby affecting their emission behaviours through the restriction of intramolecular motion.[58,99] The light-induced conversion of *trans*-assemblies from classical vesicles to porous vesicles offers intriguing opportunities for controlled permeability, drug release, and cargo transport, underscoring the potential of stereochemistry as a design element for functional AIE-active polymersomes.

Applications of AIE-active polymersomes

Catalytic potential of AIE-active polymersomes

Aggregation-induced emission (AIE)-active polymersomes exhibit a unique combination of photophysical and supramolecular features that render them suitable for photochemical catalysis. A key characteristic of many AIE luminogens is their enhanced radiative and non-radiative decay channels in the aggregated state, which not only increases fluorescence but also facilitates intersystem crossing (ISC) to triplet excited states. These triplet states can participate in energy- or electron-transfer processes to molecular oxygen, generating reactive oxygen species (ROS) such as singlet oxygen and superoxide.[100–102] While ROS generation has been primarily leveraged for photodynamic therapy, the underlying photoredox capability inherently positions AIEgens as photocatalytic units capable of mediating redox transformations under light irradiation.

The polymersome structure further amplifies this catalytic functionality by providing a nanoscale compartment with well-defined hydrophobic/hydrophilic domains. When AIE luminogens are covalently embedded in the hydrophobic membrane or core, they maintain strong emission and ROS productivity even at high local concentrations, effectively circumventing the aggregation-caused quenching (ACQ) that hampers traditional aromatic photosensitizers. Meanwhile, the hydrated corona and membrane permeability permit selective diffusion of small molecular substrates while restricting or excluding larger macromolecules, giving rise to catalytic confinement effects analogous to artificial organelles.[103] This combination of photochemical activity + confinement + selective permeability enables AIE-active polymersomes to operate as synthetic photocatalytic nanoreactors.

Photobiocatalysis has recently emerged as an attractive approach for green synthesis, integrating photocatalytic redox chemistry with enzymatic catalysis to achieve tandem transformations under mild conditions, often with solar or visible light as the sole energy input.[104–107] In these systems, nicotinamide cofactors NADH and NAD^+ function as molecular electron shuttles between photoactive units and enzymatic pathways, and their regeneration efficiency strongly dictates reaction turnover.[108,109] However, conventional photocatalysts generally produce ROS under aerobic conditions, which rapidly denature enzymes and severely restrict practical utility. Compartmentalization strategies—such as core–shell organosilica architectures—have been developed to physically isolate photocatalysis from enzymes, though such systems often rely on multi-step fabrication and lack modularity for scalable processing.[29,110,111] Amphiphilic AIE-active block copolymers offer a compelling solution owing to their intrinsic ability to

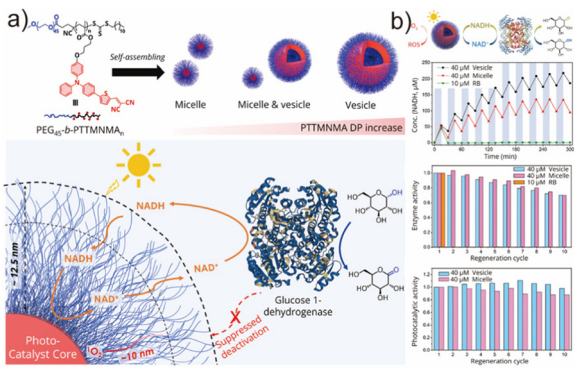

Fig. 5 (a) The depiction of the chemical structure of TTMN-based AIE block copolymers and their self-assembled micelle and vesicle architectures, and the schematic of an aerobic photobiocatalytic tandem system in water, combining the micelle/vesicle photocatalyst with glucose 1-dehydrogenase and (b) the NAD^+ regeneration catalysed by polymeric vesicles or micelles. Adapted with permission from ref. 114. Copyright 2023 America Chemical Society.

self-assemble into nanostructures such as micelles and vesicles and their capacity to encode photocatalytic AIEgens directly into the hydrophobic domains.[112,113]

To illustrate this concept, Li *et al.* introduced aggregation-induced emission (AIE)-active copolymer nanostructures as functional photobiocatalytic scaffolds (Fig. 5a).[114] Using RAFT polymerization, a series of copolymers with hydrophobic AIE blocks of increasing length (degree of polymerization: 8, 14, and 21) were synthesized and assembled *via* nanoprecipitation into micelles or vesicles, with morphology governed by packing considerations. The AIE blocks served not only as fluorophores but also as photosensitizers that remained catalytically active in the aggregated state, thus circumventing ACQ. The hydrophobic core or membrane acted as a nanoreactor for photocatalytic NADH → NAD^+ oxidation, while the hydrophilic corona excluded large enzyme molecules but permitted unhindered diffusion of the small nicotinamide cofactor (Fig. 5a). Owing to the short lifetime and diffusion radius of ROS, the hydrated shell effectively acted as a kinetic ROS barrier, intercepting and neutralizing ROS before they could reach the enzyme in bulk solution. This spatially decoupled design addressed the longstanding issue of enzyme deactivation in aerobic photobiocatalysis, enabling repeated cycling without significant performance loss. After ten operational cycles, the enzyme retained >70% of its initial activity, while the AIE micelles and vesicles preserved 85% and 98% of photocatalytic performance, respectively, indicating efficient and sustained NADH → NAD^+ turnover (Fig. 5b). Such polymeric nanoreactors highlight how AIE chemistry—originally explored in optical materials—can be strategically repurposed to solve interfacial incompatibilities at the photocatalysis–biocatalysis boundary. The modularity, aqueous compatibility, and operational robustness of these systems position them as promising candidates for scale-up and potential industrial photobiocatalytic processes.

Nanomotor potential of AIE-active polymersomes

One of the major technological challenges in nanomedicine lies in constructing nanoscale carriers with autonomous, non-Brownian motion to enhance deep tissue penetration and improve drug delivery efficiency.[115–117] Nanomotors, which convert chemical, enzymatic, or physical stimuli into directed motion, have emerged as a versatile solution to this challenge.[118,119] Their propulsion typically arises from asymmetric catalytic reactions or gradients generated on the nanoparticle surface, resulting in phoretic forces that break symmetry at the nanoscale.[120–122] Therefore, engineering nanoparticles with intrinsic morphological or chemical anisotropy has become a key strategy to design efficient nanomotor platforms. In this context, our group developed a series of Aggregation-Induced Emission (AIE) active polymersomes exhibiting intrinsically asymmetric morphologies.[123] These asymmetric vesicles, reminiscent of cucurbit-shaped structures, were fabricated *via* the precise synthesis of AIE-containing block copolymers. Specifically, we synthesized amphiphilic deblock copolymers through the ring-opening polymerization

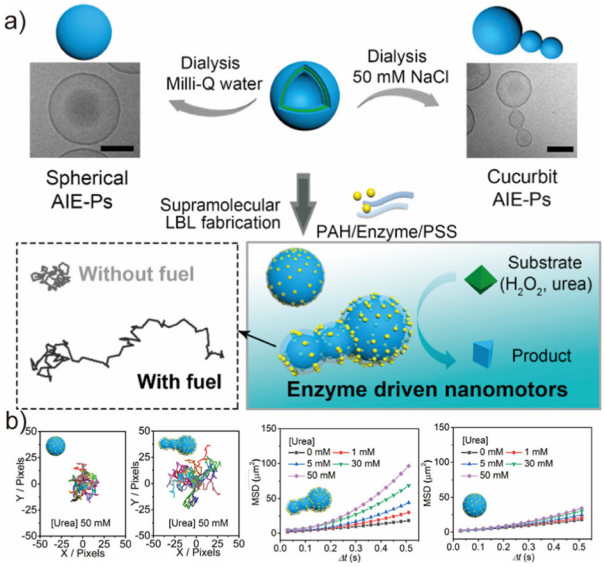

Fig. 6 (a) The schematic depiction of the enzyme-powered cucurbit-shaped AIE-polymersome nanomotors. (b) The characterization of fluorescent polymersome-based enzyme-driven AIE-nanomotors. Adapted with permission under a Creative Commons CC-BY-NC-ND 4.0 license from ref. 124. Copyright 2021 America Chemical Society.

(ROP) of 1,3-dioxane-5-carboxylic acid and 5-methyl-2-oxo-2,3,4,5,6-pentafluorophenyl ester (TMCP), followed by post-modification to introduce AIEgenic functionality.[124] Owing to the high controllability of the ROP process, the ultimate morphology of the self-assembled polymersomes was finely regulated by tuning both the AIE block length and the ionic strength during dialysis (Fig. 6a). As the length of the hydrophobic AIE block increased from 5 to 14 repeat units, the morphology evolved from spherical vesicles to cucurbit-shaped, then prolate, and ultimately tubular structures under a NaCl concentration of 50 mM. This morphology evolution can be understood from the energetic interplay between osmotic pressure and membrane-bending mechanics. During dialysis, a large osmotic energy ($E_{osmotic} \gg E_{bending}$) is generated across the polymersome membrane due to differential solute concentrations, driving rapid water efflux and substantial volume reduction. To accommodate this volume loss, the membrane undergoes deformation, selecting morphological pathways (prolate *vs.* oblate) based on the spontaneous curvature (C_0) of the bilayer. When the polymer composition imposes positive curvature, the system preferentially elongates toward tube-like or cucurbit-type structures, resulting in asymmetric vesicles with non-centrosymmetric geometry.

Leveraging this intrinsic morphological anisotropy, our group further exploited these cucurbit-like AIE-polymersomes as nanomotor scaffolds by immobilizing urease selectively on their surfaces. Urease catalyzes the hydrolysis of urea to generate ammonia and carbon dioxide, producing local chemical gradients around the polymersome. Due to the asymmetric distribution of urease, these gradients are stronger on one side of the vesicle, creating unbalanced diffusion-phoretic forces

that drive autonomous propulsion. As demonstrated in mean squared displacement (MSD) analysis, cucurbit-like polymersomes exhibited significantly higher motility compared to their spherical counterparts (Fig. 6a), confirming the role of morphology-induced asymmetry in enhancing nanomotor performance. Overall, the integration of AIE-active segments, osmotic-pressure-guided morphological programming, and enzymatic propulsion illustrates a conceptual framework for constructing functional, anisotropic nanomotors. This system not only expands the application scope of AIEgenic polymersomes beyond imaging and therapy but also highlights their potential in active drug delivery, biosensing, and other biologically relevant microenvironments.

Besides utilizing biochemical reactions for propulsion, physical stimuli present another major driving mechanism for achieving autonomous nanoscale motion. In particular, external electromagnetic fields, light, or thermal gradients can generate localized asymmetries on nanocarriers to induce motion through phoretic mechanisms. Building on this concept, our group developed a series of biocompatible AIEgenic polycarbonate-based amphiphilic copolymers with tunable hydrophobic segment lengths *via* ROP and post-modification, followed by nanoprecipitation to yield well-defined polymersomes (Fig. 7a).[125] To impart photocatalytic functionality with enhanced reactive oxygen species (ROS) production and a large two-photon absorption cross section, the tetraphenylethylene–dicyanovinyl (TPEDC) moiety was introduced as an AIEgenic side group. To enable motion, a thin gold (Au) coating was selectively deposited onto one hemisphere of the polymersomes, giving rise to a Janus configuration capable of asymmetric heat generation upon two-photon near-infrared (TP-NIR) excitation. Under 760 nm TP-NIR irradiation, the hemispherical Au layer acted as a photothermal transducer, while the underlying TPEDC segments could also absorb at ~380 nm (*via* two-photon excitation) to further contribute to heat generation through energy transfer to the Au layer (Fig. 7b). This dual excitation route significantly enhanced the thermal gradient across the nanomotor surface. MSD tracking confirmed that the AIE/Au Janus polymersomes displayed higher motility relative to Au-only nanomotors, validating that the energy transduction pathway amplified propulsion performance (Fig. 7b). The thermal gradient produced across the asymmetric nanomotor surface generated thermophoretic forces, which enabled phototactic cell percolation. *In vitro* penetration studies demonstrated that Au-coated polymersomes under NIR irradiation permeated significantly deeper into cellular clusters compared to the control groups (AIE polymersomes + irradiation and Au-coated polymersomes – irradiation), as quantified through intracellular DCFDA fluorescence, indicative of ROS accumulation (Fig. 7b). Once internalized, TP-NIR irradiation of the AIEgenic nanomotors triggered substantial intracellular ROS production due to the TPEDC moieties, resulting in oxidative stress-induced apoptosis. Calcein-AM staining confirmed rapid cell death, while propidium iodide (PI) assays revealed strong fluorescence localization in irradiated regions, evidencing spatially selective and light-controllable cytotoxicity (Fig. 7b). Taken together, this work represents a unique integration of AIE-active photodynamic elements with Janus thermophoretic nanomotion, yielding a multifunctional nanomotor platform with imaging, propulsion, and therapeutic capabilities. The successful realization of two-photon-triggered phototactic percolation followed by targeted photodynamic therapy highlights the potential of AIEgenic Janus nanomotors to overcome diffusion-limited transport barriers in tissues and opens new avenues in active nanomedicine.

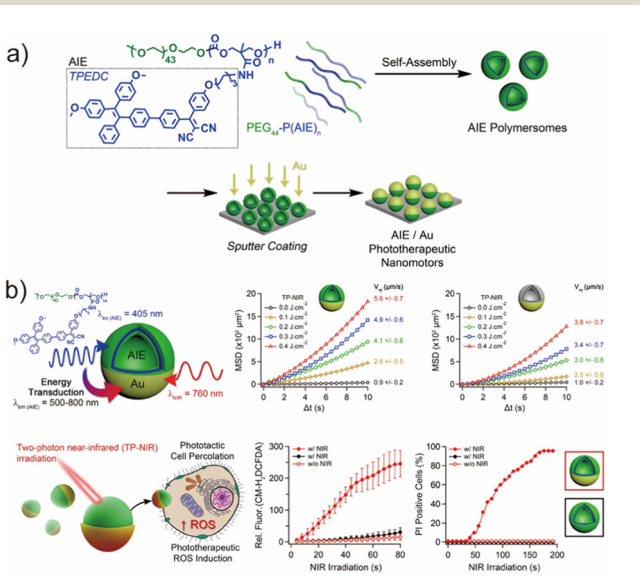

Fig. 7 (a) Design of synergistic AIE-transduced phototherapeutic nanomotors. (b) The characterization of the motility of the AIEgenic nanomotor and biological performance of this nanomotor in cancer cells. Adapted with permission under a Creative Commons CC BY license from ref. 125. Copyright 2021 Springer Nature.

Biomedical imaging utility of AIE-active polymersomes

A key advantage of aggregation-induced emission (AIE) luminogens lies in their enhanced fluorescence in the aggregated state, which fundamentally differentiates them from conventional ACQ-prone fluorophores.[126,127] This intrinsic photophysical feature makes AIEgenic polymeric vesicles and nanoparticles particularly attractive for biomedical imaging, where dense packing and nanoconfinement are unavoidable.[128–130] Besides the outstanding photophysical features of the polymersomes, the metabolic fate of the AIE polymersomes also matters a lot, when it comes to the biomedical applications. For most of the polymeric vesicles, they typically first undergo blood circulation and rapidly absorb plasma proteins to form a protein corona, which are often then recognized and cleared by the mononuclear phagocyte system, particularly in the liver and spleen.[131,132] For the biodegradable polymeric vesicles, intracellular disassembly can gradually occur under acidic, enzymatic, or redox-responsive conditions, followed ultimately by elimination through the renal or hepatobiliary pathways.[133,134] The *in vivo* metabolic fate of AIE segments is

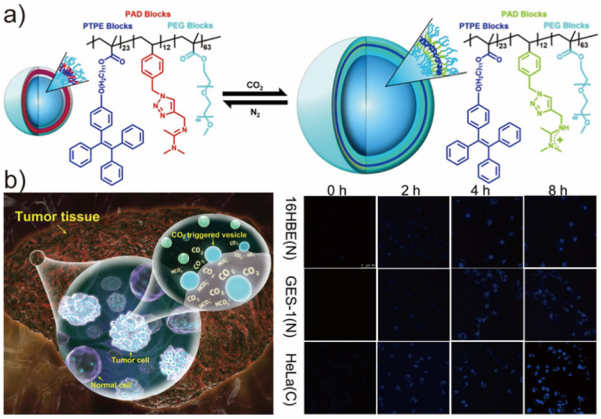

Fig. 8 (a) Illustration of the responsive process of PTPE-*b*-PAD-*b*-PEO with CO_2 and N_2. (b) The mechanism for cell imaging and the performance of the AIEgenic polymersomes for cell imaging *via* CLSM. Adapted with permission from ref. 138. Copyright 2019 America Chemical Society.

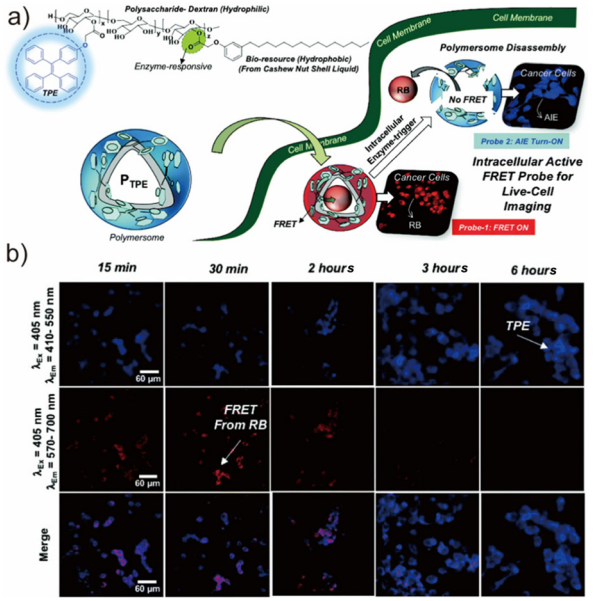

Fig. 9 (a) The scheme of the AIEgenic polymersomes and their enzyme-responsive FRET fluorescent probes for monitoring intracellular delivery in live cells and (b) the performance of polymersomes monitoring the intracellular delivery in live cells (*via* the CLSM image). Adapted with permission from ref. 139. Copyright 2021 Royal Society of Chemistry.

likewise governed by their molecular size, aggregation state, and surface characteristics.[135] Small-molecule probes are more likely to undergo hepatic and renal metabolism, whereas nanoaggregates tend to accumulate more readily in organs such as the liver and spleen before being gradually cleared.[136,137] Leveraging the properties mentioned above, Wang *et al.* synthesized a CO_2-responsive triblock copolymer – poly(4-undecoxy tetraphenyl ethylene methacrylate)-*b*-poly ((*N*-amidino)-(2,3-dihydro-1,4-methyl-1,2,3-triazole)-(ethenyl benzene))-*b*-poly(ethylene oxide) (PTPE-*b*-PAD-*b*-PEO) – *via* RAFT polymerization and subsequently fabricated fluorescent vesicles through nanoprecipitation (Fig. 8a).[138] In this design, the PAD middle block served as a chemoresponsive CO_2-recognition unit capable of undergoing reversible protonation in the presence of CO_2. This protonation converted the PAD block from hydrophobic to hydrophilic, altering the packing parameter of the amphiphile and perturbing vesicle morphology as well as the aggregation state of the TPE segments. Under continuous bubbling of CO_2, the fluorescence intensity of the vesicles initially increased due to tighter restriction of intramolecular motions in the TPE domains, and eventually reached a plateau. Upon bubbling N_2, the system was deprotonated and both fluorescence intensity and vesicle size reverted to the original state, demonstrating the reversibility of the CO_2-switchable AIE response. Importantly, tumor microenvironments typically exhibit elevated CO_2 levels due to accelerated glycolysis and high metabolic turnover in malignant tissues. Capitalizing on this physiological cue, Wang *et al.* evaluated the imaging capability of the CO_2-responsive AIE polymersomes across multiple cancer cell lines using CLSM (Fig. 8b). Minimal fluorescence was observed in normal epithelial cells (16HBE and GSE-1), while pronounced emission appeared in HeLa cervical cancer cells, 5-8F and CNE1 nasopharyngeal carcinoma cells, reflecting differential metabolic CO_2 profiles. These findings underscore the potential of CO_2-responsive AIE vesicles as tumor-selective bioimaging probes and provide a blueprint for exploiting metabolic signatures for cancer diagnostics. Beyond static bioimaging, AIE-active polymersomes can function as self-reporting nanocarriers for intracellular drug delivery due to their intrinsic fluorescence, capacity to encapsulate both hydrophilic and hydrophobic cargos, and compatibility with multiple stimulus-responsive mechanisms. An elegant example was shown by Jayakannan *et al.*, who developed enzymatically degradable AIE polysaccharide-based polymersomes composed of a hydrophilic dextran backbone and hydrophobic TPE and 3-pentadecyl phenol (PDP) substituents grafted *via* ester linkages.[139] Two model fluorescent dyes—Rose Bengal (hydrophilic) and Nile Red (hydrophobic)—were co-loaded to mimic multi-modal drug cargoes. Within cells, specific esterases cleaved the ester bonds linking the hydrophobic blocks to the backbone, triggering disassembly of the vesicles and release of the payload (Fig. 9a). Importantly, cleavage of the hydrophobic substituents disrupted the nanoscale proximity between dye molecules and AIE cores, leading to a measurable decline in fluorescence resonance energy transfer (FRET). CLSM results confirmed a substantial reduction in FRET signals within 3 h of cellular incubation (Fig. 9b), validating intracellular enzymatic activation and cargo liberation. This strategy highlights dual functionality: polymersomes serve as drug carriers while simultaneously acting as optical reporters for release dynamics, enabling visualization of intracellular pharmacokinetics in real time. Such AIE-active vesicular systems illustrate the promise of integrating therapy, imaging, and stimulus-responsiveness into modular nanoplat-

forms, thereby advancing the design of next-generation nanomedicine and bioimaging agents. Furthermore, the integration of AIE-based fluorescence imaging with other clinical modalities, such as MRI, PET, and ultrasound, offers a powerful strategy to overcome the intrinsic limitations of single-mode imaging.[140,141] Such multimodal platforms can provide complementary information, combining high sensitivity, deep tissue penetration, and quantitative capability, thereby enabling more reliable and real-time diagnostic feedback.[142,143] This synergistic approach is anticipated to further advance the biomedical applicability and clinical translation of AIE-active polymersomes.

Biomedical delivery potential of AIE-active polymersomes

The AIEgenic polymeric vesicles inherently possess the ability to encapsulate both hydrophilic molecules in their aqueous lumen and hydrophobic cargos within their membrane, making them particularly attractive as delivery vesicles in nanomedicine.[62,81,144] Beyond loading capacity, the chemical modularity of the AIEgenic copolymers—*e.g.*, tunable side-chain functionality and programmable hydrophilic–hydrophobic block ratios—enables precise regulation over vesicle size, membrane thickness, morphology, and molecular packing.[145–147] This design flexibility further allows surface engineering with targeting ligands, peptides, or responsive motifs, expanding their applicability to tumor-selective drug delivery and theranostics.

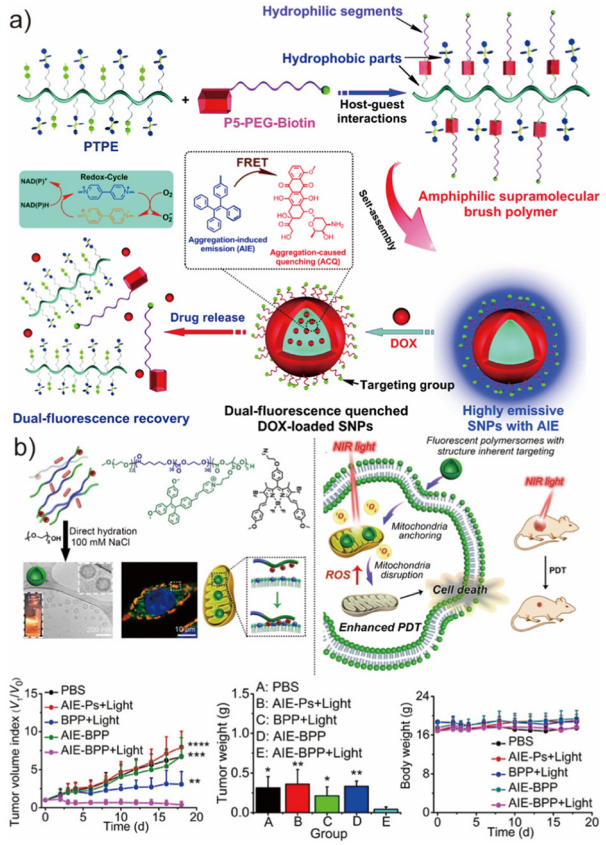

Fig. 10 (a) Schematic illustration of the formation of SNPs self-assembled from the amphiphilic supramolecular brush copolymer P5-PEG-biotin-PTPE and its use as a drug delivery vehicle. Adapted with permission from ref. 148. Copyright 2016 Royal Society of Chemistry. (b) The illustration of the biodegradable AIEgenic polymersomes *via* a salt-induced self-assembly process toward mitochondria-targeted photodynamic therapy and the performance of the polymersomes loaded with DOX applied in the PDT. Adapted with permission under a Creative Commons CC BY-NC license from ref. 149. Copyright 2021 Wiley.

Huang *et al.* developed a highly emissive supramolecular brush polymer nanoparticle system assembled through host–guest molecular recognition between a hydrophobic polystyrene-based AIE block (PTE) and a hydrophilic PEG-biotin block (P5-PEG-Biotin), the latter serving as a cancer-targeting ligand (Fig. 10a).[148] The resulting supramolecular brush polymers (SBPs) possessed low critical aggregation concentrations and a unique topological architecture conducive to stable self-assembly in aqueous media. Importantly, π–π and aromatic interactions between the TPE units and the anticancer drug doxorubicin (DOX) enhanced loading efficiency within the hydrophobic core. The system also exhibited fluorescence resonance energy transfer (FRET) between the AIE donors and DOX acceptors, allowing FRET modulation to serve as an optical readout of drug release. *In vitro* and *in vivo* studies revealed improved tumor inhibition and cell viability outcomes for DOX-loaded AIE nanoparticles relative to free DOX·HCl or PBS controls, highlighting the therapeutic promise of AIE-enabled supramolecular carriers.

Beyond cargo-dependent chemotherapy, AIEgenic polymersomes are also promising for photodynamic therapy (PDT), where cell ablation is driven by reactive oxygen species (ROS) generated from photosensitizers under light irradiation.[150] In conventional PDT, the photosensitizer must accumulate at the diseased tissue and organelle level, which is often hindered by poor targeting, photobleaching, or aggregation-caused quenching (ACQ).[151,152] The AIE framework offers clear advantages due to its enhanced emission and ROS generation in the aggregated state. van Hest *et al.* reported AIEgenic polymersomes based on biodegradable PEG-*b*-poly(caprolactone-gradient-trimethylene carbonate) (PEG-P(CLgTMC)) modified with tetraphenylethylene-pyridinium-TMC (PAIE) *via* ROP and post-functionalization (Fig. 10b).[149] Introduction of positively charged pyridinium side groups not only enhanced mitochondrial targeting through electrostatic interactions with the negatively charged mitochondrial membrane but also promoted efficient cellular uptake, aided by the nano-sized dimension (~120 nm). CLSM imaging confirmed robust internalization and indicated high cellular compatibility of the unloaded carriers.

To enable efficient ROS generation in the mitochondria, van Hest *et al.* encapsulated hydrophobic BODIPY photosensitizers within the AIEgenic vesicles, resulting in an intrinsic FRET pathway between TPE donors and BODIPY acceptors.[125] Upon NIR excitation, the nanocarriers produced abundant ROS locally within the mitochondria, leading to mitochondrial disruption and apoptotic cell death. *In vivo* studies further demonstrated that BODIPY-loaded AIE polymersomes not only

suppressed tumor progression under NIR irradiation, maintaining low tumor volume indices, but also enabled real-time fluorescence tracking of biodistribution and tumor uptake due to their intrinsic emission. This dual-function design—combining imaging, targeting, and enhanced PDT—exemplifies the powerful potential of AIE polymersomes as next-generation theranostic nanoplatforms.

In recent years, an increasing number of studies have shifted toward employing nanoparticles as carriers for photosensitizers (PSs) in photodynamic therapy (PDT).[153–155] This strategy effectively overcomes several intrinsic limitations of small-molecule PSs, such as poor aqueous solubility, non-specific biodistribution, and rapid systemic clearance. Conventional physical encapsulation of PSs into nanocarriers *via* hydrophobic interactions or van der Waals forces, however, still encounters several bottlenecks, including low drug-loading efficiency, burst leakage during circulation, and dilution-induced disassembly *in vivo*. To address these challenges, covalent conjugation of PSs to polymer scaffolds has emerged as a promising approach, enabling significantly enhanced loading capacity, minimized uncontrolled leakage, and improved formulation stability under physiological conditions. Despite these advances, most traditional PS-loaded nanoparticles suffer from low photodynamic efficiency due to aggregation-caused quenching (ACQ) of the photosensitizing moieties. Dense packing of planar aromatic chromophores in the hydrophobic core suppresses exciton diffusion and inter-system crossing, thereby reducing reactive oxygen species (ROS) generation—ultimately restricting the efficacy of PDT in cellular and *in vivo* settings. The emergence of aggregation-induced emission (AIE) photosensitizers offers a powerful solution to circumvent ACQ. Upon aggregation, AIEgens undergo restriction of intramolecular motions that boost fluorescence and enhance ROS generation, making them particularly attractive for constructing next-generation phototherapeutic nanoplatforms. Li *et al.* reported one representative example of AIEgenic vesicles formed from an amphiphilic block copolymer comprising a biodegradable poly(amino acid) backbone, hydrophilic polypropylene glycol, and hydrophobic AIE-active moieties (Fig. 11a).[156] In this design, the poly(amino acid) segments served not only as a structural bridge but also imparted excellent biocompatibility, reduced cytotoxicity, and favorable biodegradability under physiological environments—properties favorable for PDT applications both *in vitro* and *in vivo*. They further confirmed efficient fluorescence activation of the polymersome assemblies *via* Hoechst 33342 staining and confocal imaging. Interestingly, however, no significant cytotoxicity difference was observed between illuminated and non-illuminated AIEgenic polymersomes, as shown in Fig. 11b. This outcome indicated insufficient PDT efficacy despite the AIE-active photophysical behavior. Mechanistic analysis suggested that the lack of cellular internalization was the primary limiting factor; only minimal amounts of polymersomes were internalized into cancer cells, preventing effective ROS-mediated apoptosis. Li's group proposed that incorporating cationic residues, peptide ligands, or tumor-targeting moieties into the hydrophilic corona could significantly enhance endocytosis and improve PDT performance. Although the observed therapeutic outcome did not meet expectations, this study provided an important proof-of-concept demonstration—highlighting the feasibility and advantages of integrating AIE photosensitizers into polymersome nanocarriers. More importantly, it revealed key design criteria for future AIEgenic polymersomes for PDT, including (i) enhanced cellular uptake, (ii) efficient lysosomal/endosomal escape, (iii) optimized ROS generation, and (iv) tumor-targeted accumulation. With

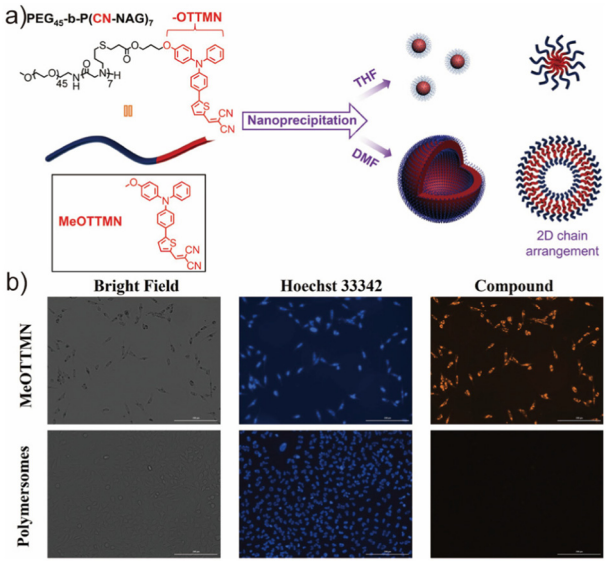

Fig. 11 (a) Illustration of the self-assembly process of PEG45-*b*-P(CN-NAG)$_7$ under different solution conditions and (b) the PDT outcomes of the AIEgenic polymersomes in the cancer cells. Adapted with permission from ref. 156. Copyright 2023 Wiley.

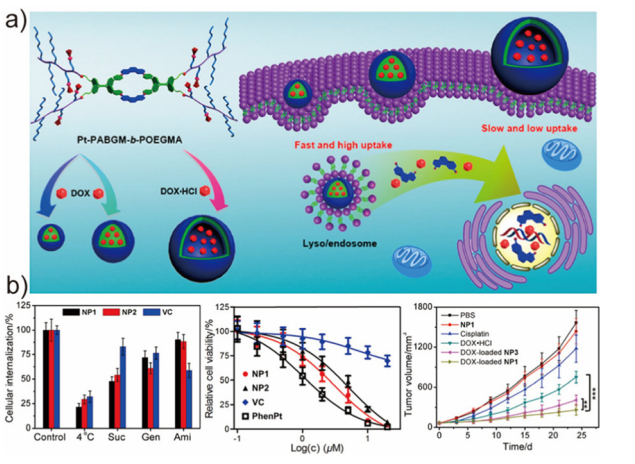

Fig. 12 (a) The illustration of the cellular uptake of DOX-loaded nanostructures self-assembled from Pt-PAZMB-*b*-POEGMA and (b) the anti-tumor performance of the polymersomes loaded with DOX *in vivo* and *in vitro*. Adapted with permission from ref. 164. Copyright 2017 America Chemical Society.

rational molecular engineering, AIEgenic polymersome platforms are expected to evolve into highly potent nano-phototherapeutics with broader translational potential.

Biomedical theranostics of polymersomes with aggregation-induced emission

Aggregation-induced emission (AIE)-active amphiphilic block copolymers have recently attracted considerable attention as multifunctional building blocks for theranostic nanoplatforms.[157–159] Their intrinsic fluorescence enables real-time tracking, while their hydrophobic domains allow efficient loading of photosensitizers or chemotherapeutics.[160,161] Such AIEgenic polymersomes therefore represent a promising class of nanocarriers for biomedical imaging and therapy.[162,163] Stang *et al.* reported one representative system in which an amphiphilic block copolymer, Pt-PAZMB-*b*-POEGMA, was synthesized *via* RAFT polymerization and subsequently conjugated with a metallacycle core (M) through an amination reaction (Fig. 12a).[164] In this design, the metallacycle M served as a highly emissive AIE-active scaffold, while the glutathione (GSH)-responsive Pt-PAZMB arms endowed the resulting supramolecular assembly with redox-triggered disassembly. Due to their amphiphilic nature, the deblock copolymers self-assembled into nanoparticles (NP1 and NP2) or vesicles (VC) using reprecipitation, dialysis, and double-emulsion techniques, respectively. The size and morphology of these nanostructures markedly influenced cellular internalization efficiency, intracellular trafficking, and cytotoxicity toward HeLa cells. These results suggested that endocytic pathways are highly sensitive to the geometric configuration of nanocarriers. Leveraging the intrinsic emission of the AIEgenic assemblies, the authors evaluated cellular uptake pathways without additional dyes. Uptake of all nanostructures was confirmed to be energy dependent (Fig. 12b), and small nanoparticles were primarily internalized through a clathrin-mediated pathway, undergoing endo-/lysosomal trafficking. In contrast, vesicles predominantly entered cells *via* macropinocytosis, which was verified through fluorescence colocalization seen between the AIEgenic vesicles and LysoTracker Red shown in confocal microscopy images.

An additional observation highlighted a major practical advantage of using AIE fluorophores in biological applications. Compared with conventional fluorescent dyes that suffer from photobleaching and aggregation-induced quenching, the AIE-active supramolecular assemblies exhibited significantly superior photostability, suggesting strong potential as next-generation fluorescent probes for long-term cellular imaging and diagnostic monitoring. Beyond diagnosis, the incorporation of GSH-responsive linkages endowed the nanocarriers with a tumor-relevant stimulus-triggered drug release behavior. Upon exposure to intracellular GSH, the Pt-PAZMB segments underwent elimination reactions, leading to the release of encapsulated doxorubicin (DOX). *In vivo* studies demonstrated pronounced tumor growth inhibition in mice treated with DOX-loaded AIEgenic nanocarriers compared to the control groups (Fig. 12b), confirming their therapeutic potential in tumor suppression. Collectively, this work highlights a valuable molecular blueprint for constructing supramolecular AIEgenic nanocarriers for theranostic applications. By integrating self-assembly, AIE-based fluorescence, redox-responsive drug release, and morphology-dependent cellular uptake, Peter *et al.* provided new insights and methodologies for the rational design of next-generation drug delivery systems (DDSs) and paved the way for future biomedical applications of AIEgenic polymersomes.

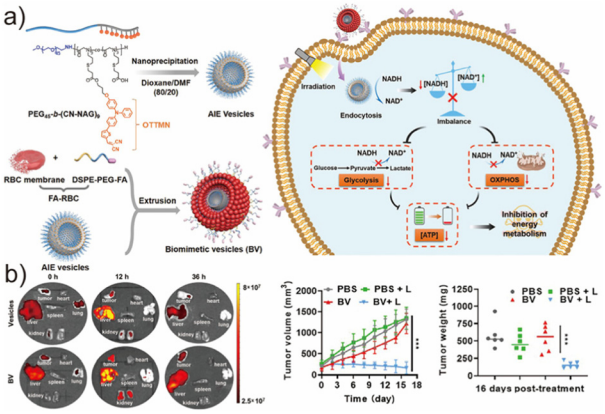

Fig. 13 (a) The preparation scheme of the AIE vesicle-based biomimetic vesicles (BV) and the mechanism of BV's tumor-targeting process. (b) The distribution of BV and the antitumor performance of the AIE-polymersomes *in vivo*. Adapted with permission from ref. 168. Copyright 2025 America Chemical Society.

Beyond photodynamic therapy (PDT), AIEgenic polymersomes can also mediate tumor suppression through photocatalytic disruption of cellular metabolism, achieving a distinct modality of theranostics.[165–167] Li *et al.* developed a biomimetic AIE polymersome nanoenzyme (biomimetic vesicles, BV) by integrating AIE-active polymeric vesicles with red blood cell (RBC) membranes (Fig. 13a).[168] The RBC membrane coating endowed the nanovesicles with superior biocompatibility, prolonged blood circulation, and reduced immune clearance, qualifying them for *in vitro* and *in vivo* tumor studies. Unlike PDT, which relies on oxygen-dependent ROS generation, BV exerted therapeutic effects *via* photocatalytic regulation of intracellular redox homeostasis. Mechanistically, under light irradiation, BV catalyzed the conversion of NADH to NAD^+, thereby perturbing the NAD^+/NADH balance, a central regulator of glycolysis and oxidative phosphorylation (OXPHOS). Disruption of this redox equilibrium inhibited both glycolytic flux and mitochondrial respiration, ultimately blocking ATP production and triggering apoptosis. Importantly, the photocatalytic NADH oxidation proceeded efficiently even under hypoxic environments, contrasting with conventional PDT, whose efficacy is severely compromised by oxygen deficiency in solid tumors. Consistently, NAD^+ yield experiments revealed similar catalytic activity for BV under air and argon conditions, confirming oxygen-independent photocatalysis. To further evaluate metabolic consequences, cytotoxicity assays demonstrated that BV exhibited significantly

enhanced cancer cell killing upon irradiation, as evidenced by a reduced IC_{50}. In parallel, intracellular ATP quantification showed a marked decrease in the ATP_light/ATP_dark ratio relative to the controls, indicating severe impairment of cellular energy metabolism. Notably, the RBC membrane coating also improved cellular uptake and biosafety compared to bare AIE polymersomes, as reflected by stronger intracellular fluorescence signals in 4T1 cells observed *via* confocal laser scanning microscopy (CLSM). *In vivo* fluorescence imaging revealed that BV preferentially accumulated in tumor tissues and liver following systemic administration (Fig. 13b). In a subcutaneous 4T1 tumor model, intravenously injected BV combined with irradiation significantly suppressed tumor growth, validating the therapeutic feasibility of metabolic intervention using metal-free photocatalytic polymersomes (Fig. 13b). Taken together, this strategy represents a compelling complement to traditional PDT. Instead of relying on exogenous cytotoxic drugs or ROS-mediated photodamage, the BV system selectively targets tumor bioenergetics by manipulating NAD^+/NADH homeostasis. Their work expands the therapeutic landscape of AIEgenic polymersomes from photodynamic and drug-mediated therapies toward metabolic disruption-based oncotherapy, offering a new paradigm for light-controlled cancer theranostics.

Despite the promising advances in AIE-active polymersomes for theranostic applications, their clinical translation still faces several challenges.[169] Like other polymeric nanomedicines, issues related to large-scale reproducibility, long-term biosafety, pharmacokinetics, and batch-to-batch consistency remain critical concerns. In addition, regulatory approval requires rigorous evaluation of their complexity, stability, and *in vivo* behaviours.[133,170] To date, although several polymer-based nanocarriers have entered clinical trials, very few have achieved clinical approval, highlighting the gap between laboratory research and clinical application. Therefore, addressing these regulatory and translational barriers will be essential for the future development of AIE-based polymersomes.

Conclusion and perspective

Aggregation-induced emission (AIE) has provided powerful new design principles for engineering emissive, multifunctional polymeric vesicles. By integrating AIE luminogens into the vesicular framework, AIE-active polymersomes overcome the aggregation-caused quenching (ACQ) that traditionally limits fluorescent polymer nanostructures, enabling robust emission in confined and densely packed environments. The synergy between the vesicular topology, featuring compartmentalization, membrane tunability, and dual cargo encapsulation, and the aggregation-tolerant photophysics of AIEgens has led to the emergence of a versatile class of nanomaterials suitable for bioimaging, controlled delivery, photodynamic therapy, and integrated theranostic modalities. Recent advances in molecular engineering, supramolecular assembly, and polymer synthesis have further enabled precise control over polymersome size, morphology, membrane permeability, photophysical characteristics, and functional output, collectively illustrating the vast biomedical potential of AIE-functional polymersome systems. Despite these achievements, several key scientific and technological challenges remain before AIE-active polymersomes can transition from proof-of-concept demonstrations to clinically relevant tools. From a materials standpoint, the development of biodegradable, metabolizable, and immuno-stealth polymer backbones, alongside AIEgens with well-defined metabolic pathways and clearance behaviors, will be crucial for biological translation. The ability to achieve structural uniformity, scalable production, and long-term physicochemical stability remains limited, and regulatory-relevant parameters, such as batch reproducibility, pharmacokinetics, biodistribution, immunogenicity, and biosafety, have not yet been systematically evaluated. On a mechanistic level, a deeper understanding of AIE chromophore behavior within dynamic and heterogeneous polymer membranes, as well as the interplay between emission, membrane mechanics, and biological microenvironments, remains largely unexplored.

Looking ahead, we anticipate future progress to move beyond passive fluorescence toward adaptive, interactive, and intelligent polymersomes. Incorporation of stimulus-responsive elements (*e.g.*, light, pH, redox, enzymatic cues, hypoxia, or mechanical stress) may enable spatiotemporal control over assembly, molecular diffusion, ROS output, or cargo release. The convergence of AIEgen-based polymersomes with emerging paradigms—such as artificial cells, biomimetic organelle engineering, immune-modulating nanomaterials, deep-tissue optical manipulation, metabolic intervention, and precision nanomedicine—may further broaden their functional landscape. Moreover, the integration of multimodal platforms that couple fluorescence with ultrasound, MRI, PET, or photoacoustic modalities could support real-time tracking and quantitative feedback, strengthening their role in clinical oncology and personalized treatment. Ultimately, the translation of AIE-active polymersomes into practical biomedical technologies will require close collaboration across polymer chemistry, photophysics, cell biology, immunology, and clinical medicine. With continued interdisciplinary efforts, we expect that AIE-enabled vesicular nanotechnology will not only address current limitations in fluorescence-based imaging and therapy but also reshape the design logic of next-generation functional biomaterials for diagnosis, therapeutic intervention, and beyond.

Author contributions

All authors contributed to the writing and revision of the manuscript.

Conflicts of interest

The authors declare no competing financial interest.

Data availability

This article is a Perspective and does not contain any original data. All information is based on the published literature, which is cited accordingly.

Acknowledgements

This work was financially supported by the National Natural Science Foundation of China (52403198), the State Key Laboratory of Advanced Polymer Materials (Grant No. sklapm2025-2-01), the National Key R&D Program of China (2024YFA1212300), and the Fundamental Research Funds for the Central Universities.

References

1 M. Lazzari and M. A. López-Quintela, *Adv. Mater.*, 2003, **15**, 1583–1594.
2 F. H. Schacher, P. A. Rupar and I. Manners, *Angew. Chem., Int. Ed.*, 2012, **51**, 7898–7921.
3 C. L. Lu and M. W. Urban, *Prog. Polym. Sci.*, 2018, **78**, 24–46.
4 J. Song, P. Huang, H. Duan and X. Chen, *Acc. Chem. Res.*, 2015, **48**, 2506–2515.
5 H. Liu, H.-H. Lu, Y. Alp, R. Wu and S. Thayumanavan, *Prog. Polym. Sci.*, 2024, **148**, 101765.
6 R. Hu, N. L. C. Leung and B. Z. Tang, *Chem. Soc. Rev.*, 2014, **43**, 4494–4562.
7 S. Varlas, S. B. Lawrenson, L. A. Arkinstall, R. K. O'Reilly and J. C. Foster, *Prog. Polym. Sci.*, 2020, **107**, 101278.
8 H. Dau, G. R. Jones, E. Tsogtgerel, D. Nguyen, A. Keyes, Y.-S. Liu, H. Rauf, E. Ordonez, V. Puchelle, H. B. Alhan, C. Zhao and E. Harth, *Chem. Rev.*, 2022, **122**, 14471–14553.
9 U. C. Palmiero, M. Sponchioni, N. Manfredini, M. Maraldi and D. Moscatelli, *Polym. Chem.*, 2018, **9**, 4084–4099.
10 Y. M. Zhao, Y. Wu, G. W. Yan and K. Zhang, *RSC Adv.*, 2014, **4**, 51194–51200.
11 R. S. M. Rikken, H. Engelkamp, R. J. M. Nolte, J. C. Maan, J. C. M. van Hest, D. A. Wilson and P. C. M. Christianen, *Nat. Commun.*, 2016, **7**, 12606.
12 C. K. Wong, A. F. Mason, M. H. Stenzel and P. Thordarson, *Nat. Commun.*, 2017, **8**, 1240.
13 I. A. B. Pijpers, S. Cao, A. Llopis-Lorente, J. Zhu, S. Song, R. R. M. Joosten, F. Meng, H. Friedrich, D. S. Williams, S. Sánchez, J. C. M. van Hest and L. K. E. A. Abdelmohsen, *Nano Lett.*, 2020, **20**, 4472–4480.
14 X. Li, Y. Wang and Q. Yan, *Angew. Chem., Int. Ed.*, 2023, **62**, e202305290.
15 R. B. Grubbs and Z. Sun, *Chem. Soc. Rev.*, 2013, **42**, 7436–7445.
16 M. C. M. van Oers, F. P. J. T. Rutjes and J. C. M. van Hest, *J. Am. Chem. Soc.*, 2013, **135**, 16308–16311.
17 H. X. Liu, H. H. Lu, Y. Alp, R. L. Wu and S. Thayumanavan, *Prog. Polym. Sci.*, 2024, **148**, 101765.
18 Q. R. Tian, C. H. Fei, H. Y. Yin and Y. J. Feng, *Prog. Polym. Sci.*, 2019, **89**, 108–132.
19 L. K. E. A. Abdelmohsen, D. S. Williams, J. Pille, S. G. Ozel, R. S. M. Rikken, D. A. Wilson and J. C. M. van Hest, *J. Am. Chem. Soc.*, 2016, **138**, 9353–9356.
20 H. Che, B. C. Buddingh' and J. C. M. van Hest, *Angew. Chem., Int. Ed.*, 2017, **56**, 12581–12585.
21 H. Che and J. C. M. van Hest, *J. Mater. Chem. B*, 2016, **4**, 4632–4647.
22 R. P. Brinkhuis, F. Rutjes and J. C. M. van Hest, *Polym. Chem.*, 2011, **2**, 1449–1462.
23 J. Hahn, S. Ding, J. Im, T. Harimoto, K. W. Leong and T. Danino, *Nat. Rev. Bioeng.*, 2024, **2**, 120–135.
24 Y. C. Chen, Y. C. Su and S. R. Roffler, *Nat. Rev. Bioeng.*, 2025, **3**, 742–760.
25 L. Schoonen and J. C. M. van Hest, *Adv. Mater.*, 2016, **28**, 1109–1128.
26 J. X. Shao, S. P. Cao, D. S. Williams, L. Abdelmohsen and J. C. M. van Hest, *Angew. Chem., Int. Ed.*, 2020, **59**, 16918–16925.
27 L. M. P. E. van Oppen, L. K. E. A. Abdelmohsen, S. E. van Emst-de Vries, P. L. W. Welzen, D. A. Wilson, J. A. M. Smeitink, W. J. H. Koopman, R. Brock, P. H. G. M. Willems, D. S. Williams and J. C. M. van Hest, *ACS Cent. Sci.*, 2018, **4**, 917–928.
28 E. Rideau, R. Dimova, P. Schwille, F. R. Wurm and K. Landfester, *Chem. Soc. Rev.*, 2018, **47**, 8572–8610.
29 R. J. R. W. Peters, M. Marguet, S. Marais, M. W. Fraaije, J. C. M. van Hest and S. Lecommandoux, *Angew. Chem., Int. Ed.*, 2014, **53**, 146–150.
30 J. Bresseleers, M. Bagheri, C. Lebleu, S. Lecommandoux, O. Sandre, I. A. B. Pijpers, A. F. Mason, S. Meeuwissen, C. F. van Nostrum, W. E. Hennink and J. C. M. van Hest, *Polymers*, 2020, **12**, 2572.
31 R. Bleul, R. Thiermann and M. Maskos, *Macromolecules*, 2015, **48**, 7396–7409.
32 F. Wang, J. Xiao, S. Chen, H. Sun, B. Yang, J. Jiang, X. Zhou and J. Du, *Adv. Mater.*, 2018, **30**, 1705674.
33 R. Peters, M. Marguet, S. Marais, M. W. Fraaije, J. C. M. van Hest and S. Lecommandoux, *Angew. Chem., Int. Ed.*, 2014, **53**, 146–150.
34 G. D. Fu, G. L. Li, K. G. Neoh and E. T. Kang, *Prog. Polym. Sci.*, 2011, **36**, 127–167.
35 A. Guinart, M. Korpidou, D. Doellerer, G. Pacella, M. C. A. Stuart, I. A. Dinu, G. Portale, C. Palivan and B. Feringa, *Proc. Natl. Acad. Sci. U. S. A.*, 2023, **120**, e2301279120.
36 R. J. R. W. Peters, I. Louzao and J. C. M. van Hest, *Chem. Sci.*, 2012, **3**, 335–342.
37 X. Wang, C. Yao, G. Zhang and S. Liu, *Nat. Commun.*, 2020, **11**, 1524.
38 Y. Luo, H. Wu, X. Zhou, J. Wang, S. Er, Y. Li, P. L. W. Welzen, R. A. J. F. Oerlemans, L. K. E. A. Abdelmohsen, J. Shao and J. C. M. van Hest, *J. Am. Chem. Soc.*, 2023, **145**, 20073–20080.

39 H. Han, S. Song, J. Wang, T. Ivanov, D. Zhou, H. Su, K. Landfester and S. Cao, *Angew. Chem., Int. Ed.*, 2026, **65**, e17620.
40 Z. Li, S. Wang, Y. Ma, J. C. M. van Hest and H. Che, *Angew. Chem., Int. Ed.*, 2026, **65**, e22097.
41 S. Feng, Y. Ma, Z. Li, S. Wang, L. Zhao, J. Lee and H. Che, *Macromolecules*, 2025, **58**, 5772–5781.
42 J. Zhang, H. Gong, C. Chen, Z. Huang, J. Xu, M. Tian, Z. Fan, C. Li and J. Du, *Adv. Funct. Mater.*, 2026, **36**, e10537.
43 H. Han, S. Song, Y. Pu, T. Ivanov and S. Cao, *Biomacromolecules*, 2026, **27**, 87–111.
44 S. Cao, P. Zhou, G. Shen, T. Ivanov, X. Yan, K. Landfester and L. C. da Silva, *Nat. Commun.*, 2025, **16**, 2407.
45 P. P. Ghoroghchian, P. R. Frail, K. Susumu, D. Blessington, A. K. Brannan, F. S. Bates, B. Chance, D. A. Hammer and M. J. Therien, *Proc. Natl. Acad. Sci. U. S. A.*, 2005, **102**, 2922–2927.
46 M. Chen and M. Yin, *Prog. Polym. Sci.*, 2014, **39**, 365–395.
47 M. Elsabahy, G. S. Heo, S.-M. Lim, G. Sun and K. L. Wooley, *Chem. Rev.*, 2015, **115**, 10967–11011.
48 S. Basu and N. Amdursky, *ACS Nano*, 2025, **19**, 33717–33733.
49 G. B. Bodedla, X. J. Zhu and W. Y. Wong, *Aggregate*, 2023, **4**, e330.
50 Z. Q. Guo, C. X. Yan and W. H. Zhu, *Angew. Chem., Int. Ed.*, 2020, **59**, 9812–9825.
51 J. Y. Mao, S. X. Ye, Y. Yang, C. J. Lu, X. L. Sun, H. Xue and W. M. Wan, *Polym. Chem.*, 2025, **16**, 3432–3442.
52 B. N. G. Giepmans, S. R. Adams, M. H. Ellisman and R. Y. Tsien, *Science*, 2006, **312**, 217–224.
53 N. Porzberg, K. Gries and K. Johnsson, *Annu. Rev. Biochem.*, 2025, **94**, 29–58.
54 L. Motiei and D. Margulies, *Acc. Chem. Res.*, 2023, **56**, 1803–1814.
55 G. S. Attar, V. Bhalla and M. Kumar, in *Encyclopedia of Aggregation-Induced Emission*, ed. B. Z. Tang, Z. Zhao and Z. Qiu, Springer Nature Singapore, Singapore, 2025, pp. 1–18. DOI: 10.1007/978-981-97-1574-9_158-1.
56 P. B. Han, H. Xu, Z. F. An, Z. Y. Cai, Z. X. Cai, H. Chao, B. Chen, M. Chen, Y. Chen, Z. G. Chi, S. T. Dai, D. Ding, Y. P. Dong, Z. Y. Gao, W. J. Guan, Z. K. He, J. J. Hu, R. Hu, Y. X. Hu, Q. Y. Huang, M. M. Kang, D. X. Li, J. S. Li, S. Z. Li, W. L. Li, Z. Li, X. L. Lin, H. Y. Liu, P. Y. Liu, X. D. Lou, C. Lu, D. G. Ma, H. L. Ou, J. Ouyang, Q. Peng, J. Qian, A. J. Qin, J. M. Qu, J. B. Shi, Z. G. Shuai, L. H. Sun, R. Tian, W. J. Tian, B. Tong, H. L. Wang, D. Wang, H. Wang, T. Wang, X. Wang, Y. C. Wang, S. Z. Wu, F. Xia, Y. J. Xie, K. Xiong, B. Xu, D. P. Yan, H. B. Yang, Q. Z. Yang, Z. Y. Yang, L. Z. Yuan, W. Z. Yuan, S. Q. Zang, F. Zeng, J. J. Zeng, Z. Zeng, G. Q. Zhang, X. Y. Zhang, X. P. Zhang, Y. Zhang, Y. F. Zhang, Z. J. Zhang, J. Zhao, Z. Zhao, Z. H. Zhao, Z. J. Zhao and B. Z. Tang, *Prog. Chem.*, 2022, **34**, 1–130.
57 F. Y. Zhu, L. J. Mei, R. Tian, C. Li, Y. L. Wang, S. L. Xiang, M. Q. Zhu and B. Z. Tang, *Chem. Soc. Rev.*, 2024, **53**, 3350–3383.
58 J. Mei, N. L. C. Leung, R. T. K. Kwok, J. W. Y. Lam and B. Z. Tang, *Chem. Rev.*, 2015, **115**, 11718–11940.
59 S. Xu, Y. Yuan, X. Cai, C.-J. Zhang, F. Hu, J. Liang, G. Zhang, D. Zhang and B. Liu, *Chem. Sci.*, 2015, **6**, 5824–5830.
60 Y. Q. Wang, B. Z. Xia, Q. N. Huang, T. Luo, Y. Y. Zhang, P. Timashev, W. S. Guo, F. Z. Li and X. J. Liang, *Adv. Healthcare Mater.*, 2021, **10**, 2100945.
61 W. H. Xu, D. Wang and B. Z. Tang, *Angew. Chem., Int. Ed.*, 2021, **60**, 7476–7487.
62 X. L. Cai and B. Liu, *Angew. Chem., Int. Ed.*, 2020, **59**, 9868–9886.
63 S. P. Cao, J. X. Shao, L. Abdelmohsen and J. C. M. van Hest, *Aggregate*, 2022, **3**, e128.
64 X. Wang, Y. Y. Yang, Y. F. Zuo, F. Yang, H. Shen and D. C. Wu, *Chem. Commun.*, 2016, **52**, 5320–5323.
65 R. Y. Zhan, Y. T. Pan, P. N. Manghnani and B. Liu, *Macromol. Biosci.*, 2017, **17**, 1600433.
66 S. Wang, Z. Li, L. Zhao, Y. Lin and H. Che, *Biomacromolecules*, 2025, **26**, 1251–1259.
67 Z. Li, B. Z. Tang and D. Wang, *Adv. Mater.*, 2024, **36**, 2406047.
68 Q. T. H. Shubhra, R. Musiol, H. C. Pan, Q. Cai, X. S. He and X. J. Cai, *Aggregate*, 2025, **6**, e70143.
69 H. C. Shen, C. H. Xu, F. Y. Sun, M. Y. Zhao, Q. Wu, J. Y. Zhang, S. J. Li, J. Zhang, J. W. Y. Lam and B. Z. Tang, *ChemMedChem*, 2022, **17**, e202100578.
70 Y. Q. Zhu, B. Yang, S. Chen and J. Z. Du, *Prog. Polym. Sci.*, 2017, **64**, 1–22.
71 R. R. Hu, Y. Kang and B. Z. Tang, *Polym. J.*, 2016, **48**, 359–370.
72 N. Zhang, Y. Fan, H. Chen, S. Trépout, A. Brûlet and M.-H. Li, *Polym. Chem.*, 2022, **13**, 1107–1115.
73 D. J. Keddie, *Chem. Soc. Rev.*, 2014, **43**, 496–505.
74 G. K. K. Clothier, T. R. Guimaraes, S. W. Thompson, J. Y. Rho, S. Perrier, G. Moad and P. B. Zetterlund, *Chem. Soc. Rev.*, 2023, **52**, 3438–3469.
75 X. He, B. Wang, X. Li and J. Dong, *RSC Adv.*, 2019, **9**, 28102–28111.
76 Z. Huang, R. Wang, Y. Chen, X. Liu, K. Wang, L. Mao, K. Wang, J. Yuan, X. Zhang, L. Tao and Y. Wei, *Polym. Chem.*, 2019, **10**, 2162–2169.
77 P. Y. Gu, C. J. Lu, F. L. Ye, J. F. Ge, Q. F. Xu, Z. J. Hu, N. J. Li and J. M. Lu, *Chem. Commun.*, 2012, **48**, 10234–10236.
78 Z. Zhang and N. Hadjichristidis, *ACS Macro Lett.*, 2018, **7**, 886–891.
79 J. Dong, R. Jiang, W. Wan, H. Ma, H. Huang, Y. Feng, Y. Dai, H. Ouyang, X. Zhang and Y. Wei, *Appl. Surf. Sci.*, 2020, **508**, 144799.
80 N. Zhang, H. Chen, Y. Fan, L. Zhou, S. Trépout, J. Guo and M.-H. Li, *ACS Nano*, 2018, **12**, 4025–4035.
81 Z. K. Li, S. B. Chen, W. H. Binder and J. T. Zhu, *ACS Macro Lett.*, 2023, **12**, 1384–1388.
82 L. Q. Liu, X. Wang, L. J. Wang, L. Q. Guo, Y. B. Li, B. Bai, F. Fu, H. G. Lu and X. W. Zhao, *ACS Appl. Mater. Interfaces*, 2021, **13**, 19668–19678.

83 R. H. Yang, Y. Wang, W. Y. Luo, Y. C. Jin, Z. Zhang, C. D. Wu and N. Hadjichristidis, *Macromolecules*, 2019, **52**, 8793–8802.
84 J. J. Sun, S. Fransen, X. Q. Yu and D. Kuckling, *Polym. Chem.*, 2018, **9**, 3287–3296.
85 J. L. Gu, F. H. Duan, S. D. Liu, W. H. Cha and J. Lu, *Chem. Rev.*, 2024, **124**, 1247–1287.
86 X. Xu, Y. Wang, Z. Li, X.-B. Zhang and G. Song, *Nat. Protoc.*, 2026, **21**, 1574–1596.
87 X. Tao, H. Chen, S. Trépout, J. Cen, J. Ling and M.-H. Li, *Chem. Commun.*, 2019, **55**, 13530–13533.
88 A. Zhang, J. Hao, S. Hou, G. Shi, Y. He, Z. Cui, M. Liu, X. Qiao, P. Fu and X. Pang, *J. Polym. Res.*, 2022, **29**, 127.
89 F. D'Agosto, J. Rieger and M. Lansalot, *Angew. Chem., Int. Ed.*, 2020, **59**, 8368–8392.
90 L. Fan, Z. Zeng, R. Zhu, A. Liu, H. Che and M. Huo, *Chem. Mater.*, 2022, **34**, 6408–6419.
91 A. Shahrokhinia, S. Rijal, B. S. Baghirzade, R. A. Scanga, P. Biswas, S. Tafazoli, O. G. Apul and J. F. Reuther, *Macromolecules*, 2022, **55**, 3699–3710.
92 S. Zhou, M. Zeng, Y. L. Liu, X. F. Sui and J. Y. Yuan, *Macromol. Rapid Commun.*, 2022, **43**, 2200010.
93 L. K. E. A. Abdelmohsen, M. Nijemeisland, G. M. Pawar, G.-J. A. Janssen, R. J. M. Nolte, J. C. M. van Hest and D. A. Wilson, *ACS Nano*, 2016, **10**, 2652–2660.
94 M. G. Jeong, J. C. M. van Hest and K. T. Kim, *Chem. Commun.*, 2012, **48**, 3590–3592.
95 X. Li, X. Liang, C. Yang and Q. Yan, *Nat. Commun.*, 2024, **15**, 8699.
96 L. Chen, J. Xiang, Y. Zhao and Q. Yan, *J. Am. Chem. Soc.*, 2018, **140**, 7079–7082.
97 D. Zhang, Y. Fan, H. Chen, S. Trépout and M.-H. Li, *Angew. Chem., Int. Ed.*, 2019, **58**, 10260–10265.
98 H. Chen, Y. Fan, X. Yu, V. Semetey, S. Trépout and M.-H. Li, *ACS Nano*, 2021, **15**, 884–893.
99 Z. Zhao, H. Zhang, J. W. Y. Lam and B. Z. Tang, *Angew. Chem., Int. Ed.*, 2020, **59**, 9888–9907.
100 J. Y. Gong, L. X. Liu, C. B. Li, Y. M. He, J. Yu, Y. Zhang, L. N. Feng, G. Y. Jiang, J. G. Wang and B. Z. Tang, *Chem. Sci.*, 2023, **14**, 4863–4871.
101 J. T. Chen, W. Li, R. L. Chen, T. F. Xie, J. X. Zhang, J. H. Chen, X. L. Sui, P. F. Zhang and J. H. Chen, *Chem. Commun.*, 2026, **62**, 2247–2250.
102 H. R. Qin, J. B. Huang, H. Liang and J. Lu, *ACS Appl. Mater. Interfaces*, 2021, **13**, 5668–5677.
103 S. Cao, T. Ivanov, J. Heuer, C. T. J. Ferguson, K. Landfester and L. C. da Silva, *Nat. Commun.*, 2024, **15**, 39.
104 W. Harrison, X. Q. Huang and H. M. Zhao, *Acc. Chem. Res.*, 2022, **55**, 1087–1096.
105 R. T. Sun, P. Chen, S. Z. Xu, L. Q. Lu and W. J. Xiao, *Angew. Chem., Int. Ed.*, 2025, **64**, e202502489.
106 Z. Q. Xing, F. L. Liu, J. Q. Feng, L. Yu, Z. P. Wu, B. B. Zhao, B. Chen, H. Ping, Y. Y. Xu, A. K. Liu, Y. Zhao, C. Y. Wang, B. J. Wang and X. Q. Huang, *Nature*, 2025, **637**, 1118–1123.
107 Y. Yuan, M. Li, W. Harrison, Z. Zhang and H. Zhao, *Nat. Catal.*, 2026, **9**, 62–72.
108 L. G. Lee and G. M. Whitesides, *J. Am. Chem. Soc.*, 1985, **107**, 6999–7008.
109 J. Kim, S. H. Lee, F. Tieves, D. S. Choi, F. Hollmann, C. E. Paul and C. B. Park, *Angew. Chem., Int. Ed.*, 2018, **57**, 13825–13828.
110 B. C. Ma, L. C. da Silva, S.-M. Jo, F. R. Wurm, M. B. Bannwarth, K. A. I. Zhang, K. Sundmacher and K. Landfester, *ChemBioChem*, 2019, **20**, 2593–2596.
111 S.-M. Jo, K. A. I. Zhang, F. R. Wurm and K. Landfester, *ACS Appl. Mater. Interfaces*, 2020, **12**, 25625–25632.
112 W. Wei, F. Mazzotta, I. Lieberwirth, K. Landfester, C. T. J. Ferguson and K. A. I. Zhang, *J. Am. Chem. Soc.*, 2022, **144**, 7320–7326.
113 S. Rodríguez-Jiménez, H. Song, E. Lam, D. Wright, A. Pannwitz, S. A. Bonke, J. J. Baumberg, S. Bonnet, L. Hammarström and E. Reisner, *J. Am. Chem. Soc.*, 2022, **144**, 9399–9412.
114 N. Zhang, S. Trépout, H. Chen and M.-H. Li, *J. Am. Chem. Soc.*, 2023, **145**, 288–299.
115 S. Hermanová and M. Pumera, *Nanoscale*, 2018, **10**, 7332–7342.
116 A. D. Fusi, Y. D. Li, A. Llopis-Lorente, T. Patino, J. C. M. van Hest and L. Abdelmohsen, *Angew. Chem., Int. Ed.*, 2023, **62**, e202214754.
117 J. L. Yong, A. S. Mellick, J. Whitelock, J. S. Wang and K. Liang, *Adv. Mater.*, 2023, **35**, 2205746.
118 S. Palagi and P. Fischer, *Nat. Rev. Mater.*, 2018, **3**, 113–124.
119 K. K. Dey and A. Sen, *J. Am. Chem. Soc.*, 2017, **139**, 7666–7676.
120 D. A. Wilson, R. J. M. Nolte and J. C. M. van Hest, *Nat. Chem.*, 2012, **4**, 268–274.
121 D. A. Wilson, B. de Nijs, A. van Blaaderen, R. J. M. Nolte and J. C. M. van Hest, *Nanoscale*, 2013, **5**, 1315–1318.
122 S. Song, H. Han, J. Wang, Y. Pu, J. Shao, J. Xie, H. Che, J. C. M. van Hest and S. Cao, *Chem. Sci.*, 2025, **16**, 7106–7129.
123 J. Shao, Y. Luo, H. Wu, J. Wang, X. Zhou, S. Er, S. Cao, H. Sun, H. H. P. Garza, H. Zheng, H. Friedrich, L. K. E. A. Abdelmohsen and J. C. M. van Hest, *Nat. Commun.*, 2025, **16**, 2445.
124 S. Cao, H. Wu, I. A. B. Pijpers, J. Shao, L. K. E. A. Abdelmohsen, D. S. Williams and J. C. M. van Hest, *ACS Nano*, 2021, **15**, 18270–18278.
125 S. Cao, J. Shao, H. Wu, S. Song, M. T. De Martino, I. A. B. Pijpers, H. Friedrich, L. K. E. A. Abdelmohsen, D. S. Williams and J. C. M. van Hest, *Nat. Commun.*, 2021, **12**, 2077.
126 H. Sun, L. K. Li, R. H. Guo, Z. Wang, Y. H. Guo, Z. L. Li and F. L. Song, *Chem. Sci.*, 2024, **15**, 940–952.
127 B. Wang, S. Liu, X. Liu, R. Hu, A. Qin and B. Z. Tang, *Adv. Healthcare Mater.*, 2021, **10**, 2101067.
128 M. Virmani, N. U. Deshpande, S. Pathan and M. Jayakannan, *ACS Polym. Au*, 2022, **2**, 181–193.

129 S. H. C. Askes, W. Pomp, S. L. Hopkins, A. Kros, S. Wu, T. Schmidt and S. Bonnet, *Small*, 2016, **12**, 5579–5590.
130 J. L. Davis, Y. Zhang, S. J. Yi, F. F. Du, K. H. Song, E. A. Scott, C. Sun and H. F. Zhang, *Langmuir*, 2020, **36**, 2291–2299.
131 M. P. Monopoli, C. Åberg, A. Salvati and K. A. Dawson, *Nat. Nanotechnol.*, 2012, **7**, 779–786.
132 D. Peer, J. M. Karp, S. Hong, O. C. Farokhzad, R. Margalit and R. Langer, *Nat. Nanotechnol.*, 2007, **2**, 751–760.
133 E. Blanco, H. Shen and M. Ferrari, *Nat. Biotechnol.*, 2015, **33**, 941–951.
134 S. Wilhelm, A. J. Tavares, Q. Dai, S. Ohta, J. Audet, H. F. Dvorak and W. C. W. Chan, *Nat. Rev. Mater.*, 2016, **1**, 16014.
135 J. Li and K. Pu, *Chem. Soc. Rev.*, 2019, **48**, 38–71.
136 Y. Hong, J. W. Y. Lam and B. Z. Tang, *Chem. Soc. Rev.*, 2011, **40**, 5361–5388.
137 X. Gu, R. T. K. Kwok, J. W. Y. Lam and B. Z. Tang, *Biomaterials*, 2017, **146**, 115–135.
138 Y. Li, X. Wu, B. Yang, X. Zhang, H. Li, A. Umar, N. F. d. Rooij, G. Zhou and Y. Wang, *ACS Appl. Mater. Interfaces*, 2019, **11**, 37077–37083.
139 N. U. Deshpande, M. Virmani and M. Jayakannan, *Polym. Chem.*, 2021, **12**, 1549–1561.
140 Y. M. Li, H. S. Yu, Y. F. Qian, J. M. Hu and S. Y. Liu, *Adv. Mater.*, 2014, **26**, 6734–6741.
141 W. J. Ye, Y. J. Tang, J. J. Wei, G. C. Li, L. L. Zhang, H. Xu and L. Wang, *J. Nucl. Med.*, 2021, **62**, 1604.
142 M. J. Mitchell, M. M. Billingsley, R. M. Haley, M. E. Wechsler, N. A. Peppas and R. Langer, *Nat. Rev. Drug Discovery*, 2021, **20**, 101–124.
143 A. Louie, *Chem. Rev.*, 2010, **110**, 3146–3195.
144 H. D. Xu, X. Chen, H. Wang, C. Z. Wang, Y. J. Guo, Y. X. Lin, Y. H. Huang, J. Q. Hou and X. D. Wei, *Aggregate*, 2024, **5**, e580.
145 Y. Y. Bao, *Molecules*, 2021, **26**, 6267.
146 D. Ding, R. T. K. Kwok, Y. Y. Yuan, G. X. Feng, B. Z. Tang and B. Liu, *Mater. Horiz.*, 2015, **2**, 100–105.
147 Y. S. Dong, B. Liu and Y. Y. Yuan, *J. Controlled Release*, 2018, **290**, 129–137.
148 G. Yu, R. Zhao, D. Wu, F. Zhang, L. Shao, J. Zhou, J. Yang, G. Tang, X. Chen and F. Huang, *Polym. Chem.*, 2016, **7**, 6178–6188.
149 S. Cao, Y. Xia, J. Shao, B. Guo, Y. Dong, I. A. B. Pijpers, Z. Zhong, F. Meng, L. K. E. A. Abdelmohsen, D. S. Williams and J. C. M. van Hest, *Angew. Chem., Int. Ed.*, 2021, **60**, 17629–17637.
150 C. Y. Zhang, Y. Q. Shi, Z. R. Zhu, T. Yang, Y. W. Wang, S. S. Hu, Q. Wu, H. J. Yang, J. H. Liu, W. H. Zhu and Q. Wang, *ACS Nano*, 2025, **19**, 12119–12137.
151 X. H. Min, T. Fang, L. L. Li, C. Q. Li, Z. P. Zhang, X. E. Zhang and F. Li, *Nanoscale*, 2020, **12**, 2340–2344.
152 H. Y. Huang, W. S. Xie, Q. Wan, L. C. Mao, D. N. Hu, H. Sun, X. Y. Zhang and Y. Wei, *Adv. Sci.*, 2022, **9**, 2104101.
153 D. H. T. Le, V. Ibrahimova, S. A. H. van den Wildenberg, H. L. Wu, A. Fonseca, T. Torres, E. Garanger, W. P. J. Leenders, R. Brock, S. Lecommandoux and J. C. M. van Hest, *Angew. Chem., Int. Ed.*, 2023, **62**, e202300511.
154 Y. Zhang, X. Q. Zhang, H. C. Yang, L. Yu, Y. Xu, A. Sharma, P. Yin, X. Y. Li, J. S. Kim and Y. Sun, *Chem. Soc. Rev.*, 2021, **50**, 11227–11248.
155 H. Jeong, W. Park, D. H. Kim and K. Na, *Adv. Drug Delivery Rev.*, 2021, **177**, 113954.
156 Z. Zhang, H. Chen, Y. Wang, N. Zhang, S. Trépout, B. Z. Tang, G. Gasser and M.-H. Li, *Macromol. Rapid Commun.*, 2023, **44**, 2200716.
157 N. K. S. Teo, B. Fan, A. Ardana and S. H. Thang, *Aggregate*, 2024, **5**, e414.
158 X. H. Chen, H. J. Han, Z. Tang, Q. Jin and J. Ji, *Adv. Healthcare Mater.*, 2021, **10**, 2100736.
159 L. R. Wang, R. Hu, A. J. Qin and B. Z. Tang, *ChemMedChem*, 2021, **16**, 2330–2338.
160 J. P. Shi, X. Sun, L. Song, M. C. Hong, Q. Yuan and Y. Zhang, *Prog. Mater. Sci.*, 2024, **142**, 101246.
161 J. Kim, Y. Piao and T. Hyeon, *Chem. Soc. Rev.*, 2009, **38**, 372–390.
162 X. Yan, H. Wang, C. E. Hauke, T. R. Cook, M. Wang, M. L. Saha, Z. Zhou, M. Zhang, X. Li, F. Huang and P. J. Stang, *J. Am. Chem. Soc.*, 2015, **137**, 15276–15286.
163 J. B. Zhuang, B. Wang, H. Chen, K. Y. Zhang, N. Zhao, N. Li and B. Z. Tang, *ACS Nano*, 2023, **17**, 9110–9125.
164 G. Yu, M. Zhang, M. L. Saha, Z. Mao, J. Chen, Y. Yao, Z. Zhou, Y. Liu, C. Gao, F. Huang, X. Chen and P. J. Stang, *J. Am. Chem. Soc.*, 2017, **139**, 15940–15949.
165 A. Chiarugi, C. Dölle, R. Felici and M. Ziegler, *Nat. Rev. Cancer*, 2012, **12**, 741–752.
166 R. P. Goodman, A. L. Markhard, H. Shah, R. Sharma, O. S. Skinner, C. B. Clish, A. Deik, A. Patgiri, Y.-H. H. Hsu, R. Masia, H. L. Noh, S. Suk, O. Goldberger, J. N. Hirschhorn, G. Yellen, J. K. Kim and V. K. Mootha, *Nature*, 2020, **583**, 122–126.
167 D. V. Titov, V. Cracan, R. P. Goodman, J. Peng, Z. Grabarek and V. K. Mootha, *Science*, 2016, **352**, 231–235.
168 Y. Ma, Y. Deng, W. Xue, X. Ji and M.-H. Li, *J. Am. Chem. Soc.*, 2025, **147**, 26557–26572.
169 A. C. Anselmo and S. Mitragotri, *Bioeng. Transl. Med.*, 2016, **1**, 10–29.
170 J. Shi, P. W. Kantoff, R. Wooster and O. C. Farokhzad, *Nat. Rev. Cancer*, 2017, **17**, 20–37.